ANALYSIS OF CURRENT INDUCTION ON THIN CONDUCTORS INSIDE THE BODY DURING MRI SCAN

A DISSERTATION SUBMITTED TO

THE GRADUATE SCHOOL OF ENGINEERING AND SCIENCE

OF BILKENT UNIVERSITY

IN PARTIAL FULFILLMENT OF THE REQUIREMENTS FOR

THE DEGREE OF

DOCTOR OF PHILOSOPHY

IN

ELECTRICAL AND ELECTRONICS ENGINEERING

By

Volkan Açıkel

December, 2014

Analysis of current induction on thin conductors inside the body during MRI scan
By Volkan Açıkel
December, 2014

We certify that we have read this thesis and that in our opinion it is fully adequate, in scope and in quality, as a dissertation for the degree of Doctor of Philosophy.

Prof. Dr. Ergin Atalar(Advisor)

Prof. Dr. Murat Eyüboğlu

Prof. Dr. Ayhan Altıntaş

Prof. Dr. Kader Karlı Oğuz

Asst. Prof. Dr. Özgür Ergül

Approved for the Graduate School of Engineering and Science:

Prof. Dr. Levent Onural
Director of the Graduate School

ABSTRACT

ANALYSIS OF CURRENT INDUCTION ON THIN CONDUCTORS INSIDE THE BODY DURING MRI SCAN

Volkan Açıkel
Ph.D. in Electrical and Electronics Engineering
Advisor: Prof. Dr. Ergin Atalar
December, 2014

The aim of this thesis is to develop a method to analyze currents on thin conductor structures inside the body during Magnetic Resonance Imaging (MRI) scan based on Modified Transmission Line Method (MoTLiM). In this thesis, first, Active Implantable Medical Devices (AIMDs) are modeled and the tissue heating problem, which is a result of coupling between AIMD and incident Radio Frequency (RF) fields, is examined. Then, usage of MoTLiM to analyze the currents on the guidewires is shown by solving currents on guidewire when a toroidal transmit receive coil is used with guidewire.

At first, a method to measure MoTLiM parameters of leads using a network analyzer is shown. Then, IPG case and electrode are modeled with a voltage source and impedance. Values of these parameters are found using the Modified Transmission Line Method (MoTLiM) and the Methods of Moments (MoM) simulations. Once the parameter values of an electrode/IPG case model are determined, they can be connected to any lead, and tip heating can be analyzed.

To validate these models, both MoM simulations and MR experiments are used. The induced currents on the leads with the IPG case or electrode connections are solved using the proposed models and MoTLiM. These results are compared with the MoM simulations. In addition, an electrode is connected to a lead via an inductor. The dissipated power on the electrode is calculated using MoTLiM by changing the inductance and the results are compared with the specific absorption rate results that are obtained using MoM. Then, MRI experiments are conducted to test the IPG case and the electrode models. To test the IPG case, a bare lead is connected to the case and placed inside a uniform phantom. During a MRI scan the temperature rise at the lead is measured by changing the lead length. The power at the lead tip for the same scenario is also calculated using the IPG case model and MoTLiM. Then an electrode is connected to a lead via an inductor and placed inside a uniform phantom. During

a MRI scan the temperature rise at the electrode is measured by changing the inductance and compared with the dissipated power on the electrode resistance.

Second, based on the similarity between currents on guidewires and transmission lines, currents on the catheter are solved with MoTLiM. Current distributions on an insulated guidewire are solved and B_1 distribution along the catheter is calculated. Effect of stripping the tip on the tip visibility is analyzed. It is shown that there is an increase in the B_1 at the insulation and bare guidewire boundary. Then, a characteristic impedance is defined for the guidewires and impedance seen at the point where guidewire is inserted into the body is calculated. It is shown with EM simulations that if the impedance converges to the characteristic impedance of the guidewire, tip visibility of the guidewire is lost.

At last, a new method to measure electrical properties of a phantom material is proposed. This method is used for validation of the coaxial transmission line measurement (CTLM) fixture, which is designed for measurement of electrical properties of viscous phantom materials at MRI frequencies, and which is previously presented by our group. The new method depends on the phenomena of the lead tip heating inside a phantom during MRI scan. Electrical properties of a phantom are influential on the relationship between tip temperature increase and the lead length. MoTLiM is used and the relationship between the lead length and the tip temperature increase is formulated as a function of conductivity and permittivity of the phantom. By changing the lead length, the tip temperature increase is measured and the MoTLiM formulation is fitted to these data to find the electrical properties of the phantom. Afterwards the electrical properties of the phantom are measured with the CTLM fixture and the results that are obtained with both methods are compared for an error analysis.

To sum, electrical models for the IPG case and electrode are suggested, and the method is proposed to determine the parameter values. The effect of the IPG case and electrode on tip heating can be predicted using the proposed theory. An analytical analysis of guidewire with toroidal transceiver is shown. This analysis is helpful for better usage and improvements of toroidal transceiver. Also, MoTLiM analysis can be extended to other MRI guidewire antennas.

Keywords: MRI safety, implant, radio frequency, interventional mRI, device visualization, catheter antenna.

ÖZET

MRG TARAMA SIRASINDA VÜCUDUN İÇİNDEKİ İNCE İLETKENLER ÜZERİNDE OLUŞAN AKIMLARIN ANALİZİ

Volkan Açıkel
Elektrik ve Elektronik Mühendisliği, Doktora
Tez Danışmanı: Prof. Dr. Ergin Atalar
Aralık, 2014

Bu tezin amacı Manyetik Rezonans Görüntüleme (MRG) sırasında vücudun içindeki ince iletken yapılar üzerinde oluşan akımları analiz etmek için değiştirilmiş iletim hattı metoduna (MoTLiM) dayalı bir yöntem geliştirmektir. Vücuda yerleştirilebilen aktif tıbbi cihazlar modellenmiş ve bu cihazların radyo frekans alanları ile etkileşiminden kaynaklı doku ısınma problemi incelenmiştir. Ardından, MoTLiM kullanılarak toroidal alıcı verici anten kullanıldığında kılavuz teller üzerinde oluşan akımlar incelenmiştir.

İlk olarak vücuda yerleştirilen implant tellerinin MoTLiM parametrelerini ölçmek için devre çözümletici ölçümlerinin kullanıldığı bir yöntem geliştirilmiştir. Daha sonra darbe üretgeç kılıfı ve elektrot kısımları voltaj kaynağı ve empedans olarak modellenmiştir. Voltaj kaynağı ve empedans değerleri MoTLiM ve momentler metodu (MoM) benzetimleri beraber kullanılarak bulunmuştur.

Bu modelin geçerliliğini test etmek için MoM benzetimleri ve MR deneyleri kullanılmıştır. Teller üzerinde oluşan akımlar önerilen modeller ve MoTLiM kullanılarak çözülmüştür. Bu çözümler MoM benzetimlerinden elde edilen sonuçlarla karşılaştırılmıştır. Sonrasında elektrot tele bir indüktör ile bağlanmıştır. Farklı indüktör değerleri için elektrot üzerinde harcanan güç MoTLiM ve önerilen model kullanılarak hesaplanmıştır. Harcanan güç sonuçları MoM benzetimlerinden elde edilen özgül soğurma hızı değerleriyle karşılaştırılmıştır. Sonrasında önerilen devre modelleri MR deneyleri ile test edilmiştir. Darbe üretgeç kılıfını test etmek için çıplak tel kılıfa bağlanarak tekdüze jelden yapılan doku modeli içerisine yerleştirilmiştir. Tel uzunluğu değiştirilerek tel ucundaki sıcaklık artışı ölçülmüştür. Ölçülen durumlar için tel ucudaki güç MoTLiM ve devre modeli ile hesaplanmıştır. Elektrot modelinin testi için ise elektrot çıplak tele indüktör ile bağlanarak jel doku modelinin içerisinde MR cihazına yerleştirilmiştir. İndüktör değeri değiştirilerek elektrot ucundaki sıcaklık artışı ölçülmüştür. Aynı durumlar

için elektrotta harcanan güç önerilen modelle hesaplanmıştır.

İkinci olarak kılavuz telleri üzerlerinde oluşan akımların iletim hatlarındaki akımlara olan benzerliğinden faydalanarak kılavuz teller MoTLiM ile modellenmiştir. Yalıtımlı klavuz teller üzerindeki akımlar çözülmüştür ve etraflarında oluşan B_1 manyetik alan hesaplanmıştir. Kılavuz tellerin uç kısmını soymanın uç görünürlüğünü üzerindeki etkisi incelenmiştir. Soyulmuş ve yalıtımlı tel sınırında manyetik alanda artış olduğu gösterilmiştir. Daha sonra kılavuz tel için karakteristik empedans tanımlanmiştir. Telin vücuda girdiği noktadaki empedans hesaplanmiştir ve bu empedansın karakteristik empedansa ulaştığı durumlarda tel görünürlüğünün yok olduğu elektromanyetik benzetimler ile gösterilmiştir.

Son olarak da, eksendeş iletim hattı aparatı ile yapılan ölçümleri test etmek için MoTLiM tabanlı bir yöntem kullanılmıştır. Bu yeni yöntem doku modeli içerisindeki tellerin MR çekimi sırasında ısınmaya neden olmasından faydalanmaktadır. Bu ısınma, doku modelinin elektriksel özelliklerine bağlıdır. Tel uzunluğu ile ısınma arasında bir formül elde edilmiştir. Bu formül aynı zamanda doku modeli elektriksel özelliklerini de barındırmaktadır. Tel uzunluğu değiştirilerek yapılan ölçümlere bu formül uygulanarak doku modeli elektriksel özellikleri bulunmuştur ve iki yöntemden elde edilen sonuçlar karşlaştırılmıştır.

Sonuç olarak bu tezde vücuda yerleştirilebilen aktif tıbbi cihazların radyo frekans güvenliğini incelemek için bir model geliştirilmiştir. Aynı model kılavuz tellerin güvenliği için de kullanılabilir. Ayrıca bu modelin kılavuz tellerin MRI çekimi sırasındaki görünürlürlüğünün analizinde de kullanılabilineceği gösterilmiştir. Son olarak da geliştirilen model doku modeli olarak kullanılan jellerin elektriksel özelliklerini ölçmek için kullanılmış ve daha önce geliştirilmiş olan eksendeş iletim hattı aparatı test edilmiştir.

Anahtar sözcükler: MRG güvenliği, vücuda yerleştirilebilen tıbbi cihazlar, radyo frekans, girişimsel MRG.

Acknowledgement

Completion of this doctoral dissertation is in virtue of support and guidance of many people. First of all, I would like to express my sincere appreciation and gratitude to Prof. Dr. Ergin Atalar for giving me the chance to work with him. I am thankful to him for his great mentorship, and everything he thought me. I am also indebted to Prof. Dr. Ayhan Altıntaş and Prof. Dr. Murat Eyüboğlu for their guidance throughout the thesis follow up committees. I would like to express my gratitude to Asst. Prof. Dr. Özgür Ergül as well, for showing interest and using his precious time to read this thesis and giving his critical comments about it. And I am especially thankful to Prof. Dr. Kader Karlı Oğuz for participating in my defense jury.

I also want to thank to my friends from UMRAM Taner Demir, Can Kerse, Umut Gündoğdu, Cemre Arıyürek, Koray Ertan, Berk Silemek, Soheil Taraghinia, Redi Poni and Reyhan Ergün for their friendship and helps throughout this thesis work.

I am grateful to Can Uran, Aslı Ünlügedik, Akbar Alipour and Behnam Ghassemiparvin for their companionship throughout the time of this study.

Finally, I owe special gratitude to my parents and my sister for their continuous and unconditional support.

This work is partially supported by TUBITAK BIDEB scholarship number 2228.

Contents

List of Figures

List of Tables

Chapter 1

Introduction

In this thesis, a novel method of analyzing the electromagnetic properties of elongated metallic structures inside the body of a patient during the Magnetic Resonance Imaging (MRI) procedure. The novel method uses the fact that the elongated wires inside the body behaves like a transmission line. The proposed method can be helpful in understanding the radio frequency safety issues of active implantable medical devices such as pacemakers, deep brain stimulators. It can also be helpful in understanding and optimization of guidewire visibility when the method of Radio Frequency (RF) current induction on these guidewires is used for tracking the position of these instruments inside the MRI scanners. Here, first the problem of implant heating in MRI is discussed before the guidewire visibility problem.

MRI is a very powerful diagnostic tool with its high soft tissue contrast and it can be used for diagnosis of lots of diseases. MRI is widely used imaging modality in brain and nerve disease imaging. Also, MRI can provide valuable information about joint abnormalities, and abdomen. Another advantage of MRI is providing accurate information about these diseases and guide these operations without using ionized radiation. With all these superiorities MRI has increasing utilization in clinics [1]. It is reported by OECD iLibrary that there are 102.7, 97.9 and 97.4 MRI exams per population of 1000 in USA, Greece and Turkey,

respectively, during 2011 [2]. Also, there is a survey [3] undertaken for 2009 in 61 countries, and it shows that there is an increase in the number of patients who wear cardiac pacemakers. Growth in both usage of MRI and cardiac pacemakers results in possibility of $50 - 75\%$ of patients with pacemakers requires MRI scan over lifetime of the device [1].

However, patients with metallic implants cannot utilize the advantages of MRI because of the safety reasons. One of the problems with the metallic implants is coupling with RF transmit coils. This coupling may result in rise in temperature of the tissue around the electrode. Some patients who wear AIMDs cannot take advantage of MRI or can be scanned under restrictive conditions. In conventional MRI scanners, the RF fields, which are essential for MRI, are generated by birdcage body coils. The coupling between AIMDs and the body coils may result in high E-field in the tissue around AIMDs [4] and can cause excessive tissue heating [5]. The safety of the leads inside MRI scanners has been studied extensively [6, 7]. There are MRI conditional pacemakers [8] which patients with these implants can be imaged under certain conditions. But, determination of these conditions require many MRI experiments in which AIMDs are tested inside a phantom under several different configurations.

Electromagnetic simulations and phantom experiments are the most powerful tools for the safety analysis of AIMDs. Although very accurate results can be obtained using these tools, a simple model can also prove helpful for understanding the problem. Additionally, an accurate model is helpful for designing more precise experiments. For example, Carmichael et al. [9] investigated the safety of intracranial electroencephalograph (EEG) electrodes using two different tail configurations, i.e., open circuit and short circuit. However, another configuration may result in a worse case. Modeling of leads, electrodes and implantable pulse generator (IPG) cases can prove helpful for understanding the interactions between them. Nordbeck et al. [10] analyzed 36 different cases by changing electrode and lead properties and showed the interactions between different leads and electrodes. Although these results illustrate the effect of electrodes and IPG cases on implant heating, a systematic method is required to better understand the behavior of these components of AIMDs.

Nitz et al. modeled the electrodes as resistive elements [11] in their analysis of lead tip heating. However, the safety concern lies in the interaction of the implant with the RF pulse, and therefore, the analysis should be conducted at or around the Larmor frequency. In addition, a non-zero reactance in the equivalent circuit is expected. As will be shown in later parts of the thesis, an additional voltage or current source is required to accurately model the electrode and the IPG case. The model parameters must be defined in relation to the RF scattering behaviors of the lead, the electrode, and the IPG case.

In this thesis, the IPG case and electrode parts of an AIMD are modeled such that they can be used with the Modified Transmission Line Method (MoTLiM) [12]. The model of the IPG case and electrode are explained, following the method used to find the model parameters are detailed. After finding the model parameters, induced currents on leads with the IPG case or electrode connections are determined using MoTLiM. Finally, the proposed methods are tested using MRI experiments. A lead is connected to an IPG case, and by changing the lead length, the temperature rise is measured and compared with the SAR values, which are calculated using the IPG case model and MoTLiM. Additionally, an electrode is connected to a lead via an inductor, and by changing the inductance, tip heating at the electrode is measured and compared with the SAR values, which are calculated using a circuit model.

Moreover, recent advancements show MRI is also promising tool for interventional operations [13, 14]. Interventional procedures under MRI requires specialized guidewires and catheters for imaging and tracking purposes. For interventional MRI, guidewires and catheters need modification in order to be visible and safe during the MRI [4]. Loopless antenna [15], elongated loop [16], solenoids [17] are used methods to make guidewires and catheters visible inside MR image. However, using these structures comes with the cost of decreased mechanical integrity, steerability and maneuverability. Also, active coils on the catheters require connection network to scanner [16]. With these modifications RF induced tissue heating risk emerges. The RF induced tissue heating problem is one of the problems that needs to be solved before interventional MRI is used in clinics. Safety analysis of implants using MoTLiM is applicable to safetry analysis of

guidewires. Moreover, MoTLiM can be used for analysis of visibility performance of the guidewires.

Etezadi-Amoli et al. [18] showed a promising method to use conductive catheters and guidewires inside MRI with low RF power levels. Also, this method simplifies the connection of catheters and guidewires to the scanner. In their work, the toroidal coil is well investigated with extensive MRI experiments. However, its analysis was mostly experimental and no theoretical and/or analytical analysis was conducted to show its working principles. In this work, currents on the guidewire inside the body is solved using MoTLiM and how stripping the tip of the guidewire increases the B_1, which is shown by Etezadi-Amoli et al. [18] experimentally, at the tip of the guidewire is shown. Then using impedance analysis and Smith chart at some cases, tip visibility of the guidewire is lost.

Furthermore, MoTLiM is used for verification of coaxial transmission line fixture for the measurement of electrical properties of phantoms. For MRI safety studies, information of electrical properties of phantom material is crucial for accuracy of the calculations. Thus, a measurement setup that can precisely measure electrical properties of the phantom material is essential.

Dielectric properties of biological materials have been studied for a long period of time. In recent papers, there is a variety of methods for measuring electrical conductivity and permittivity. The open ended coaxial probe [19] is one of the common ways for measuring dielectric properties. In recent literature, substances measured by open ended coaxial probe include biological tissues [20], tumors [21], binary mixtures of liquids [22], particle suspensions and emulsions [23], food [24], vegetation [24], and soil [25]. However, while using open ended coaxial line, fringing fields at the open end must be handled carefully. These fringing field can easily be affected by improper contact with the Substance Under Test (SUT), leading to miscalculations. Also, for open ended coaxial measurement techniques, one needs semi-infinite materials which is hard to achieve with low loss materials at low frequencies. Transmission reflection (T/R) methods [26] can be alternative measurement techniques. However, most of the structures for T/R methods are not applicable to liquid or viscous materials. Parallel plate structures

are also among common techniques; however, these structures highly suffer from fringing fields at RF and higher frequencies. Another technique is measuring propagation constant [27]. There are several advantages and disadvantages of these techniques to be taken into account in measurement. The key disadvantage of these studies for MRI researchers is the frequency range of these methods. Most of the methods in the literature are working at microwave frequencies or at low frequencies.

In this thesis, an MRI based electrical properties measurement technique is presented for the verification of the coaxial transmission line fixture for electrical properties measurement which was presented by Akin et al [28]. For the comparison of the results obtained by both methods, Hydrocyethyl cellulose (HEC) phantoms are used. HEC phantoms are in gel form so that they can be filled into the CTL fixture and have no convection so that they can be used for MRI temperature increase experiments. The comparison of these two methods are carried out to gain confidence in measurements.

Chapter 2

Active Implantable Medical Device Modeling

2.1 Background

When a lossy body is considered, there are current loops inside the body due to the incident RF field. When a lead is placed inside the body, the patterns of these current loops change and follow a different loop, including the lead itself. Therefore, there is current flowing from the body to lead and from the lead to body along the lead. In Figure 2.1(a), the current flowing at the lead tissue boundary of the lead is shown without the IPG case. Because the lead is a source-free region, the total current flowing into and out from the lead must be zero. However, the presence of an IPG case or electrode changes these currents along the lead. In Figure 2.1(b), the current pattern at the boundary of a lead and the body is shown for a lead connected to an IPG case. It can be observed that total current at the lead and tissue boundary is not zero. However, in this case, there must be a source. To show this effect for the IPG case and electrode, a current source is used in the circuit model. Since the magnitudes of conduction and displacement currents are comparable, a complex impedance is used in order to model the interaction between the IPG case and the electrode with the tissue. Therefore,

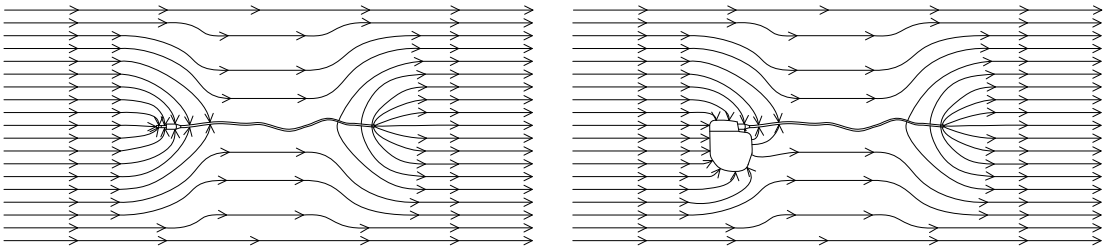

(a) (b)

Figure 2.1: (a) and (b) are sketch of the current patterns around a lead and a lead connected to a pulse generator, respectively.

the circuit model of the electrodes and IPG cases has a current source (I_c) and impedance (Z_c), as shown in Figure 2.2(a). However, to be consistent with the previous studies in the literature [11, 29] and because boundary conditions are easily defined throughout the thesis, instead of a current source and impedance, a Thevenin equivalent (V_c and Z_c), is used.

After defining the circuit models, the scattering problem can be converted into a simple circuit problem and then solved. This circuit model is easy to use with previously published model, which is based on the modified transmission line circuit model [12] as shown in Figure 2.2(b). Z is the series impedance, and Y is the shunt admittances of the lead. From the circuit model of the lead, wavenumber along the lead was defined as $k_t = \sqrt{-ZY}$.

In MoTLiM [12], the behavior of the induced currents are modeled using the second order differential equation

$$I(s) + \frac{1}{k_t^2}\frac{d^2I(s)}{ds^2} = \frac{E^i(s)}{Z}, \tag{2.1}$$

where $k_t = \sqrt{-ZY}$ is the wavenumber along the lead, Z is the distributed impedance, s is the position along the lead, $I(s)$ is the current on the lead and $E^i(s)$ is the tangential component of the incident E-field. Equation 2.1 is derived from the modified lumped element model of the lead. Using the same model, an equation for the hypothetical voltage, which is useful for defining some boundary conditions, can be derived as

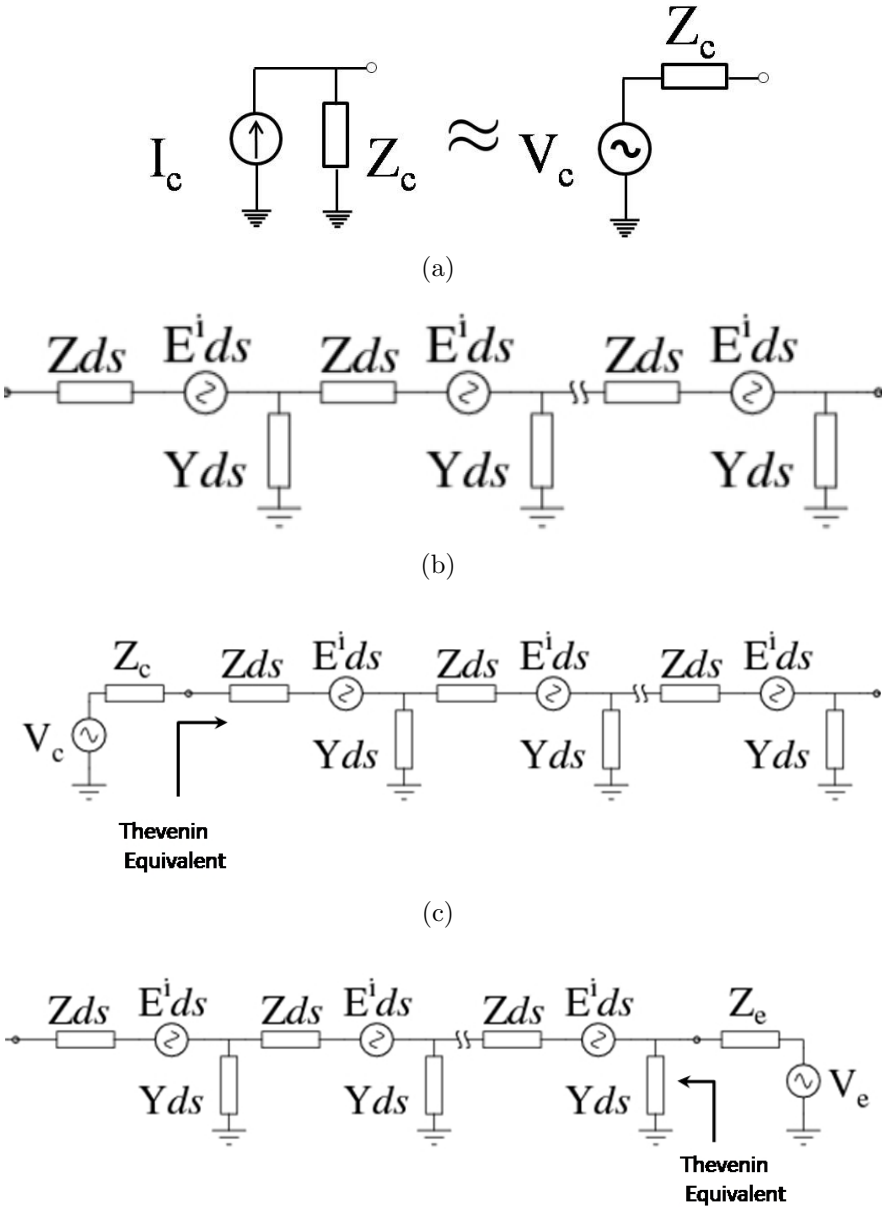

Figure 2.2: (a) The IPG case and electrode model as the current source and impedance and the Thevenin equivalent circuit. (b) The modified transmission line model. Distributed voltage sources are introduced to show the effect of the incident field. (c) The IPG case model connected to the modified transmission line model. (d) The electrode model connected to the modified transmission line model.

$$V(s) = \frac{Z}{k_t^2}\frac{dI(s)}{ds}. \tag{2.2}$$

Using the equation of continuity, it can be observed that the hypothetical voltage is the scaled version of the charge distribution along the lead. However, using the hypothetical voltage can help define associated concepts throughout the thesis. Once parameters for lead, IPG case and electrode are found induced current on the leads can be solved for any known E-field incidence.

2.2 Measurement of MoTLiM Parameters of a Lead

In our earlier study, we modeled the lead (not including its electrode or case) using MoTLiM [12]. In this model, the lead is assumed to be in a hypothetical shield. An hypothetical voltage between this shield and the lead and the current on the lead are formulated using well-known telegrapher equation. This model simplifies the lead current calculation dramatically by replacing the lead with two parameters: the serial lead impedance per length and the equivalent wave number. The relationship between the scattering properties of the lead and environment are also demonstrated. Previously these parameters are found by solving scattering problem from the lead geometry and showed for simple cases like bare straight and insulated cylindrical wires. However, leads usually have more complex geometries like helix, twisted wires and multiple insulation layers. For each different lead geometry, MoTLiM parameters of the lead must be found by solving the RF scattering problem. However, for some cases solving the RF scattering problem from the lead may be difficult. So a method to measure MoTLiM parameters of a lead is developed.

A lead is connected to inner conductor of a coaxial cable and a loopless antenna is formed as shown in Figure 2.3. When the loopless antenna, which is shown in Figure 2.3, is inserted into the lossy medium, it can be considered as two

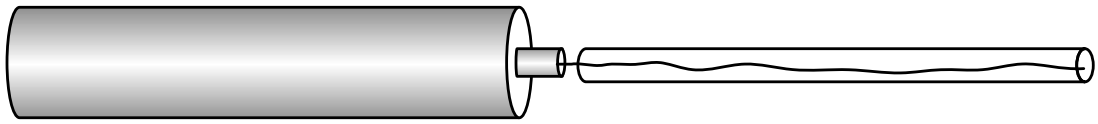

Figure 2.3: A lead is connected to inner conductor of a coaxial cable and a loopless antenna is formed.

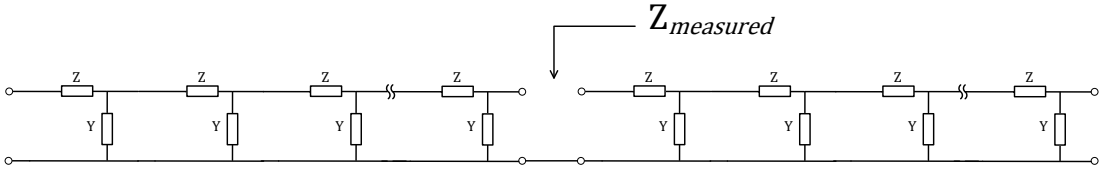

Figure 2.4: Loopless antenna can be considered as connected transmission lines.

transmission lines connected as shown in Figure 2.4. In this system one of the transmission lines is formed by the lead and the surrounding medium and the other one is the outer conductor of the coaxial line and the surrounding medium. Note that the transmission line model for the outer conductor of the coaxial line is different from the coaxial transmission line and the model parameters are different from the transmission line parameters of the coaxial line, and depend on the radius of outer conductor and the electrical properties of the surrounding medium. As there is no incident E-field, there is no voltage source in the MoTLiM model, and the traditional transmission line model can be used. So impedance on the transmission line can be found using;

$$Z_in = Z_0 \frac{Z_l + Z_0 \tanh(jk_t l)}{Z_0 + Z_l \tanh(jk_t l)}, \tag{2.3}$$

where Z_0 is the characteristic impedance of the lead and can be found as $-jZ/k_t$, which is the ratio of voltage wave to current wave traveling in the same direction.

As termination, if the both transmission lines are open circuit, Equation 2.3 can be written as

$$Z_{in} = Z_0 \coth(jk_t l), \tag{2.4}$$

Furthermore if the length of the coaxial line is long enough, Equation 2.4 converges to the characteristic impedance,Z_{0coax}, of the transmission line. So transmission line system shown in Figure 2.4 can be considered as serially connected two impedances as shown in Figure 2.5.

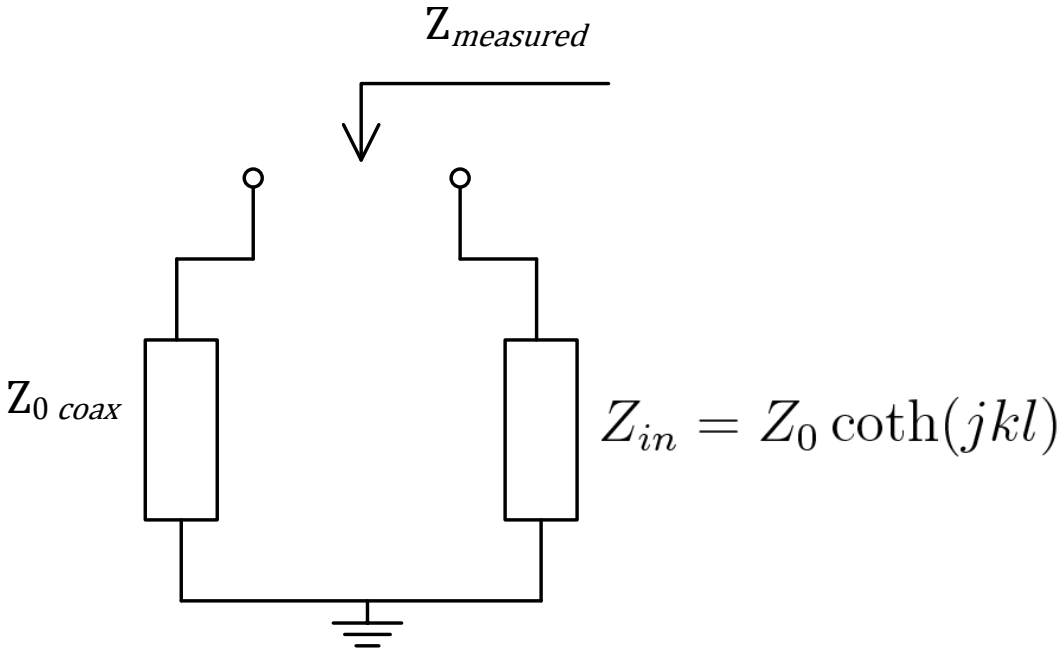

Figure 2.5: Equivalent circuit model of the transmission line system.

As outer conductor of the coaxial cable is cylindrical, its transmission line parameters inside the surrounding medium can be found analytically. Then measuring the impedance,$Z_{measured}$, shown in Figure 2.5 using a network analyzer for different lead lengths and fitting the measured data to the calculated impedance, MoTLiM parameters of the lead inside the surrounding medium can be found. However, before the measurements, calibration of the coaxial line is done outside the medium. When it is inserted into the medium, there will be an impedance between the inner and outer conductors of the coaxial line, and to correct this effect, equivalent circuit must be corrected as shown in Figure 2.6. With the correction for the phantom impedance $Z_{measured}$ can be found as

$$Z_{measured} = Z_{phantom}//(Z_{0coax} + Z_0 coth(jkl)). \tag{2.5}$$

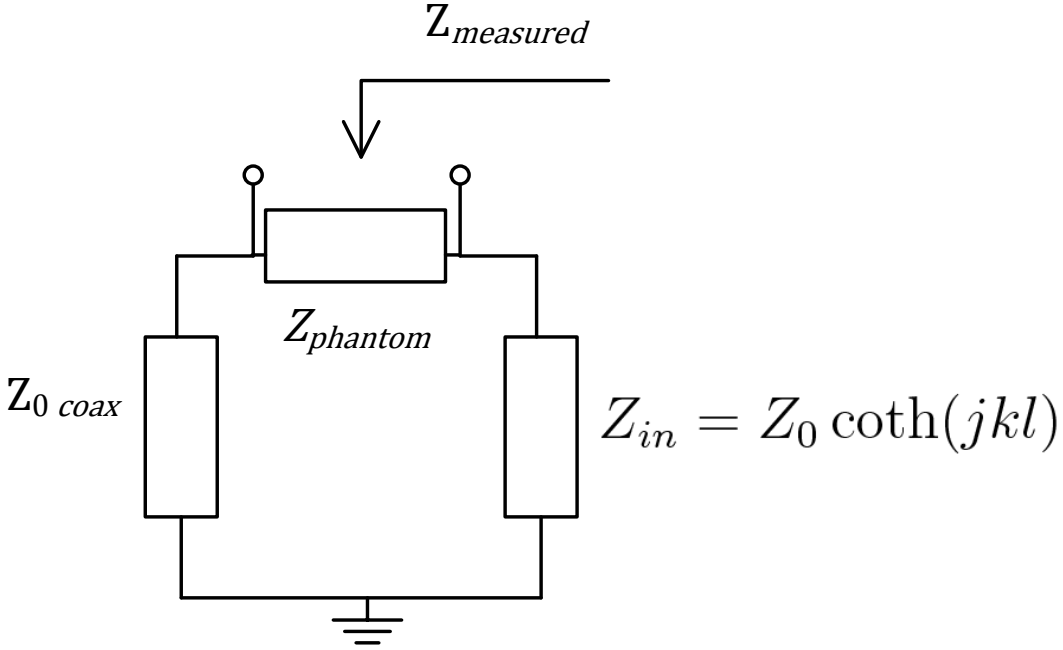

Figure 2.6: Corrected equivalent circuit model of transmission line system.

2.3 Modeling of IPG Case and Electrode

For the sake of simplicity, the proposed theory is explained using uniform E-field exposure. However, the concepts that are explained throughout the thesis can be re-derived for any known incident E-field.

2.3.1 Modeling of the IPG Case and Electrode

To explain the method, we consider an IPG case and determine its parameter values. In MoTLiM, leads are modeled as shown in Figure 2.2(b) with series impedances, Z, and shunt admittances, Y, for infinitesimally small portions of lead. First, the Thevenin equivalent of a lead is found at the point shown in Figure 2.2(c) using MoTLiM. Solving Equations 2.1 and 2.2 with a uniform E-field, the current and hypothetical voltage along the lead can be found as

$$\begin{aligned} I(s) &= Ae^{-jk_t s} + Be^{jk_t s} + \frac{E_i}{Z} \\ V(s) &= \frac{-jZ}{k_t}(Ae^{-jk_t s} - Be^{jk_t s}), \end{aligned} \tag{2.6}$$

where E_i is the tangential component of the uniform incident field, A and B are the unknowns that can be found using boundary conditions.

To find the open circuit voltage, V_{oc}, for a lead with length l_m the boundary conditions

$$\begin{aligned} I(s=0) &= 0 \\ I(s=-l_m) &= 0, \end{aligned} \tag{2.7}$$

are used in Equation 2.6 and the unknowns A and B are thus determined.

V_{oc} is found as

$$V_{oc}(s=0) = \frac{jE_i}{k_t}\frac{2\sin(k_t l_m/2)e^{jk_t l_m/2}}{\sin(k_t l_m)} - \frac{E_i}{k_t}, \tag{2.8}$$

To find the short circuit current, I_{sc}, the boundary conditions

$$\begin{aligned} V(s=0) &= 0 \\ I(s=-l_m) &= 0 \end{aligned} \tag{2.9}$$

are used in Equation 2.6, and the unknowns A and B are determined.

I_{sc} is found as

$$I_{sc}(s=0) = \frac{E_i}{Z} - \frac{E_i}{Z}\frac{1}{\cos(k_t l_m)}, \tag{2.10}$$

V_{oc} is the Thevenin voltage, and the Thevenin impedance can be found as

$$Z_{th} = \frac{V_{oc}}{I_{sc}} = \frac{Z}{k_t}\frac{4\sin(k_t l_m/2)\cos(k_t l_m)e^{jk_t l_m/2} + \sin(2k_t l_m)}{\sin(2k_t l_m) - 2\sin(k_t l_m)}. \tag{2.11}$$

Using the Thevenin equivalent of the lead and the IPG case model, Kirchhoff's voltage equation can be written as follows:

$$V_c - IZ_c - IZ_{th} - V_{th} = 0 \tag{2.12}$$

where I is the current at the connection point of the IPG case and the lead. However, in Equation 2.12, there are three unknowns. I can be found using MoM simulations, but there is still a need for a second equation to find the remaining two unknowns. Therefore, a second lead, for example with different length, can be used for these calculations, and a second Kirchhoff's voltage equation is obtained. Then, solving the Kirchhoff's voltage equations for two leads simultaneously, the parameters of the IPG case can be found.

To find the parameters of the electrode circuit model (V_e and Z_e), the same method can be applied.

2.3.2 Induced Currents on Lead with Electrode and IPG Case

Because the birdcage coils are widely used as transmit coils in MRI and they have a fairly uniform E-field distribution along their z-axis, uniform E-field exposure to the implants is not an unlikely situation. Therefore, we consider a lead under uniform E-field incidence with length $-l_m$. We connect the lead to an IPG case at position $s = 0$ and leave the other end of the lead at position $s = l_m$ floating inside the medium.

Solving Equations 2.1 and 2.2 with a uniform E-field, the current and hypothetical voltage along the lead are found, as in Equation 2.6. To find the unknowns A and B, the following boundary conditions:

$$\begin{aligned} V - I(0)Z_c - V_c &= 0 \\ I(s = l_m) &= 0 \end{aligned} \tag{2.13}$$

are applied. Where V_c is the IPG case voltage and Z_c is the IPG case impedance. The same boundary condition can be used for the electrode by replacing V_c with the electrode voltage (V_e) and Z_c with the electrode impedance (Z_e). Applying

the boundary conditions in Equation 2.13, the following equation system with two unknowns A and B can be found:

$$\begin{aligned} \frac{-jZ}{k_t}(A-B) - (A+B+\frac{E_i}{Z})Z_c - V_c &= 0 \\ Ae^{-jk_t l_m} + Be^{jk_t l_m} + \frac{E_i}{Z} &= 0 \end{aligned} \tag{2.14}$$

Solving Equation 2.14, the unknowns A and B and, consequently, the induced current and the hypothetical voltage can be found.

2.3.3 Calculation of the Rise in Tip Temperature

Circuit models of the IPG case and electrode need to be verified; however, they are not directly measurable quantities. Therefore, for the verification of the circuit models, their effect on the rise in tip temperature at the lead tip is used. Instead of calculating the rise in tip temperature directly, the square of the hypothetical voltage is used. The hypothetical voltage is the scaled version of the charge on the lead. Assuming that the scattered fields decay fast due to the conductivity of the tissue, the square of the hypothetical voltage has a linear relationship with the SAR and the rise in temperature at the lead tip.

2.3.3.1 Formulation of the Rise in Tip Temperature at the Lead Tip and Effect of the IPG Case

When an uniform E-field excitation, $E^i(s) = E_0$, is applied, the current and hypothetical voltage along the lead can be found as in Equation 2.6. Let the lead be located between $s = -l_m/2$ and $s = l_m/2$. If both ends of the lead is not connected to any IPG case or electrode, the current at $s = \pm l_m/2$ is zero. Therefore, the induced current and the hypothetical voltage along the lead can be found as

$$
\begin{aligned}
I(s) &= \frac{E_0}{Z} - 2\frac{E_0}{Z}\frac{\sin(k_t\frac{l_w}{2})}{\sin(k_t l_w)}\cos(k_t s) \\
V(s) &= 2\frac{E_0}{k_t}\frac{\sin(k_t\frac{l_w}{2})}{\sin(k_t l_w)}\sin(k_t s). \qquad (2.15)
\end{aligned}
$$

Then, at the lead tip, the square of the hypothetical voltage becomes

$$
|V|^2 = |\frac{E_0}{k_t} tan(k_t l_w/2)|^2. \qquad (2.16)
$$

Assuming that the scattered fields are decaying fast due to the loss of the surrounding medium, the hypothetical voltage has an approximate quadratic relationship with the rise in temperature at the tip of the lead ($s = l_m/2$) and can be formulated as

$$
\Delta T = C|\frac{2E_0}{k_t} tan(k_t l_w/2)|^2, \qquad (2.17)
$$

where C is a constant, which depends on thermal properties of the medium as explained in Yeung et al. [5], and includes the spatial averaging effect [30]. In this work, the value of C is not calculated and therefore the above equation is considered as a proportionality.

To see the effect of the IPG case, a lead with length l_m is connected to the IPG case at $s = 0$, and the square of the hypothetical voltage is calculated at $s = -l_m$. Under uniform E-field exposure, the hypothetical voltage distribution along the lead is found using Equation 2.6. Additionally, the unknowns A and B must be found by applying the boundary conditions

$$
\begin{aligned}
I(0) &= 0 \\
V - Z_c I(s = -l_m) - V_c &= 0, \qquad (2.18)
\end{aligned}
$$

where Z_c and V_c are the case impedance and voltage, respectively. By determining the unknowns A and B, the square of the hypothetical voltage can be found.

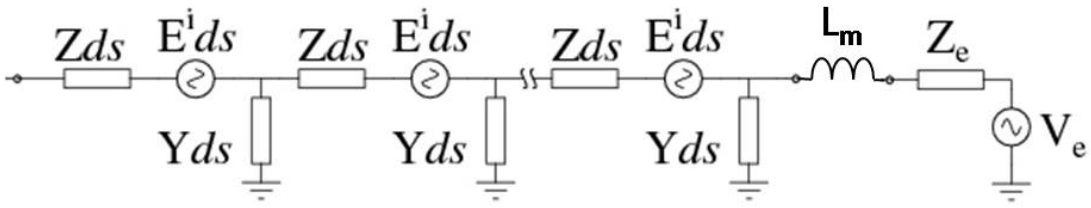

(a)

(b)

Figure 2.7: (a) Modified transmission line model connected to the electrode via a matching inductor. (b) Connection of the lead to the electrode via a matching inductor.

2.3.3.2 Effect of Matching the Lead Impedance to the Electrode Impedance

The electrode impedance indicates the interaction of the electrode with the tissue. Therefore, the dissipated power associated with the real part of the electrode impedance is the power dissipated in the tissue. From this point of view, it can be considered as the scaled version of the SAR around the electrode. Therefore, the dissipated power associated with the real part of the electrode has a linear relationship with the rise in temperature. First, the Thevenin equivalent of the lead is found, as in Equations 2.8 and 2.11 from the point shown in Figure 2.2(d). Then, using the Thevenin equivalent and the circuit model of the electrode, the dissipated power from the electrode can be approximated as

$$Re\{P_e\} = R_e(\frac{V_{th} - V_e}{Z_{th} + Z_e})(\frac{V_{th} - V_e}{Z_{th} + Z_e})^*, \tag{2.19}$$

where R_e is the real part of the electrode impedance. If a matching impedance is placed between the electrode and the lead, as shown in Figure 2.7, the dissipated power on the electrode can be calculated as

$$Re\{P_e\} = R_e(\frac{V_{th} - V_e}{Z_{th} + Z_e + Z_m})(\frac{V_{th} - V_e}{Z_{th} + Z_e + Z_m})^*. \quad (2.20)$$

Although the perfect power matching condition cannot be achieved with a single element, the imaginary part of the sum of the Thevenin impedance of the lead and the electrode impedance can be canceled out. Under this condition, the dissipated power from the electrode can be maximized. Any change in the value of the matching impedance will reduce the dissipated power.

2.4 Method

2.4.1 Measurement of MoTLiM Parameters

A bare wire with 0.55mm diameter is connected to a semi rigid coaxial cable and impedance in Figure 2.6 is measured by changing the wire length from 2cm to 30cm inside the gel phantom with electrical conductivity of 0.17S/m and 63 relative permittivity. Then an insulated wire with diameter 0.79mm and 0.0175mm insulation thickness is connected to the semi rigid coax and impedance is measured by the wire length from 2cm to 30cm inside the same gel phantom.

2.4.2 IPG Case and Electrode

The circuit model parameters of the IPG case and electrode are found using the MoTLiM and MoM together. Then, their validity is checked using the MoM simulations and MRI experiments. For the MoM simulations, FEKO is used (EM software & Systems Germany, Böbligen, GMbH), and the MRI experiments are conducted using the 3T Siemens TimTrio system.

2.4.2.1 IPG Case Circuit Model

The circuit model of the IPG case is tested using MoM simulations and MRI experiments. A rectangular box with dimensions 1.2cm ×4.4cm ×5cm, which are close to commercially available pulse generator dimensions, is used for both the simulations and experiments. For the simulations, the box is considered to be a perfect electric conductor (PEC). For the MRI experiments, a copper box is built; however, the loss of copper is ignored for the calculations. A circular phantom is prepared for the experiment and filled with HEC solution. The permittivity and conductivity of the phantom material are 55 and 0.17S/m, respectively. Phantom gel is prepared such that its electrical properties are close to electrical properties of human tissue [31].

To find the values of IPG case circuit model parameters, the method explained in Section 2.3.1 is used. Bare wires with a diameter of 0.5mm and lengths of 15 cm and 45cm are connected to the PEC box. The current at the connection point of the IPG case and wire is found using the MoM for both wire lengths. To validate the model parameter, a bare wire with a diameter of 1.3mm is connected to the PEC box, and the induced current under uniform E-field on the leads are solved for lead lengths of 40.3cm, 35.3 cm, and 27.3 cm, which are chosen to show that models are capable of solving the oscillatory behavior of the induced currents. The results are compared with the MoM simulations. During MoM simulations a lead is placed on z axis and the PEC box is connected to it. PEC box is meshed with maximum edge length of 0.5mm and leads are segmented with maximum segment length of 2mm. All geometry is illuminated by 4 plane electromagnetic waves propagating in x, $-x$, y and $-y$ directions and E-field component is in z direction to emulate the birdcage coil. The IPG case model is also tested using MRI experiments. The IPG case is connected to the bare lead with a diameter 1.3mm and positioned inside the phantom, as shown in Figure 2.8(a). This configuration ensures that the lead is exposed to a uniform E-field. The length of the lead is changed from 5.3cm to 45.4cm, and the temperature rise at the lead tip is measured using a fiber optic temperature sensor (Optical Temperature Sensor,

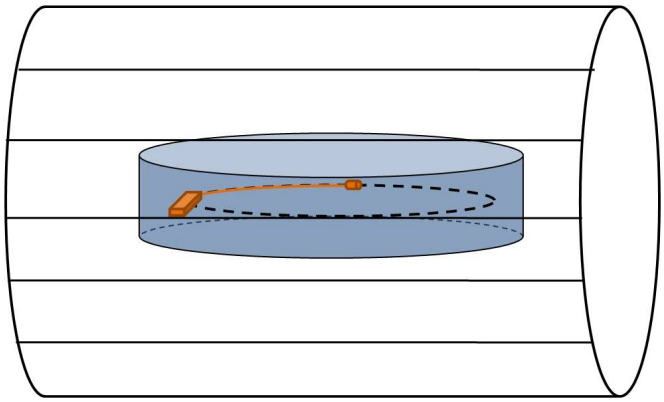

(a)

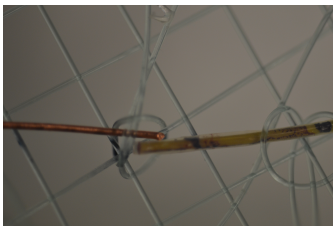

(b)

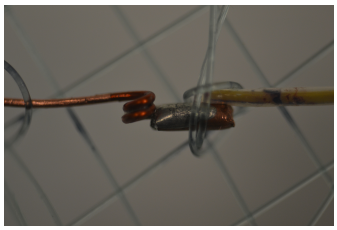

(c)

Figure 2.8: (a) The experimental setup. In all of the experiments, with the IPG case or the electrode, leads are placed on a circular path as shown, with the black circle inside the cylindrical phantom. The phantom is placed inside the MR scanner to be co-centered with the transmit body birdcage coil. (b) and (c) Placement of the temperature sensors with respect to the lead and electrode. In (c) an inductor can be seen between the lead and electrode. Setup is placed on a net formed of fishing line and fixed using knots.

Neoptix Reflex-4 RFX134A) as shown in Figure 2.8(b). The square of the hypothetical voltage at the lead tip is calculated and compared with the experimental data. Using the same lead and removing the IPG case, the experiments to measure the rise in the tip temperature are repeated by changing the lead length from 11cm to 55cm. Lead lengths are chosen to show the shift in resonance peaks.

2.4.2.2 Electrode Circuit Model

The circuit model of the electrode is also tested using both MoM simulations and MRI experiments. For the simulations, a spherical electrode with a 1mm radius

is used, and the circuit parameters inside the medium are determined to be as follows: Conductivity of 0.42S/m and relative permittivity of 81, which are close to electrical properties of human tissue [31]. The electrode is connected to bare leads with a radius of 0.5mm and lengths 10cm and 30cm. During MoM simulations; leads are positioned along the z axis and a spherical electrode is connected to them. The electrode is meshed with maximum edge length of 0.5mm and the leads are segmented with maximum segment length of 2mm. The geometry is excited with plane electromagnetic wave similar to the previous simulations. The induced currents at the connection points of the leads to the electrode are found using MoM simulations for both lead lengths. Then, the Thevenin equivalents of both the leads are found using MoTLiM, and the values of the circuit model parameters are found. Then, the spherical electrode is connected to bare leads with a radius of 0.1mm and lengths 25cm, 35cm, and 45cm. Induced currents on the leads are solved for uniform E-field incidence using the MoTLiM, and the results are compared with the MoM simulations. For the MRI experiments, using an inductor between the lead and the electrode the impedance of the electrode is matched to the Thevenin impedance of the lead. Although, perfect matching cannot be reached with single element, imaginary part of the sum of lead Thevenin impedance, electrode impedance and impedance of inductor can be adjusted to zero. A cylindrical copper electrode is used with a radius of 2.2mm and length of 7mm, which are close to dimensions of a commercial electrode. During the experiments, a gel phantom with a conductivity of 0.14S/m and relative permittivity of 60 is used. The circuit model parameters of the cylindrical electrode are found for the medium which has the same electrical properties of the phantom used during the experiments. Bare leads with a radius of 1 mm and lengths 10cm and 40cm are used. Before the experiments, a matching concept is tested using MoM simulations. The spherical electrode is connected to a bare lead with a radius of 0.1mm and length of 25cm. An inductor is placed between the electrode and the lead. The Thevenin equivalent of the bare lead is found using MoTLiM. The electrode model is connected to the Thevenin equivalent of the lead via a matching inductor. By changing the value of the inductance in the range from 1nH to 250nH, the real part of the dissipated power is calculated for the electrode impedance using the MoTLiM. Then, E-field and SAR are calculated on

the surface of the spherical electrode using MoM simulations and compared with MoTLiM simulation results.

Then, matching the lead impedance to the electrode impedance is demonstrated using experiments. A bare wire with a radius of 0.5mm and length of 20cm is connected to the cylindrical electrode with a radius of 2.2mm and length of 7mm via a custom-made matching inductor. The value of the inductance is varied from 20nH to 160nH. Lead length is chosen close to the resonance length and inductors are wound to fit inside a lead. For each inductance value, the temperature rise at the electrode is measured. For each condition, the real part of the dissipated power associated with the electrode impedance is calculated using the MoTLiM and the electrode model. These calculations are compared with the experimental data. All calculated power values are for 1V/m incident E-field; however during experiments much higher incident field is used.

2.5 Results

2.5.1 MoTLiM Parameter Measurement Results

Parameter measurements are done inside a phantom with conductivity 0.17S/m and relarive permittivity 63 for bare wire with 0.55mm diameter and for insulated wire with 0.79mm diameter and 0.0175mm insulation thickness. Figure 2.10 red dashed lines are the magnitude and phase of the measured impedance, black lines are the fitting of Equation 2.5 to the measured data for bare wire. Figure 2.10 red dashed lines are the magnitude and phase of the measured impedance, black lines are the fitting of Equation 2.5 to the measured data for insulated wire. Z and k values are found and compared with the calculated values, error is less than 6

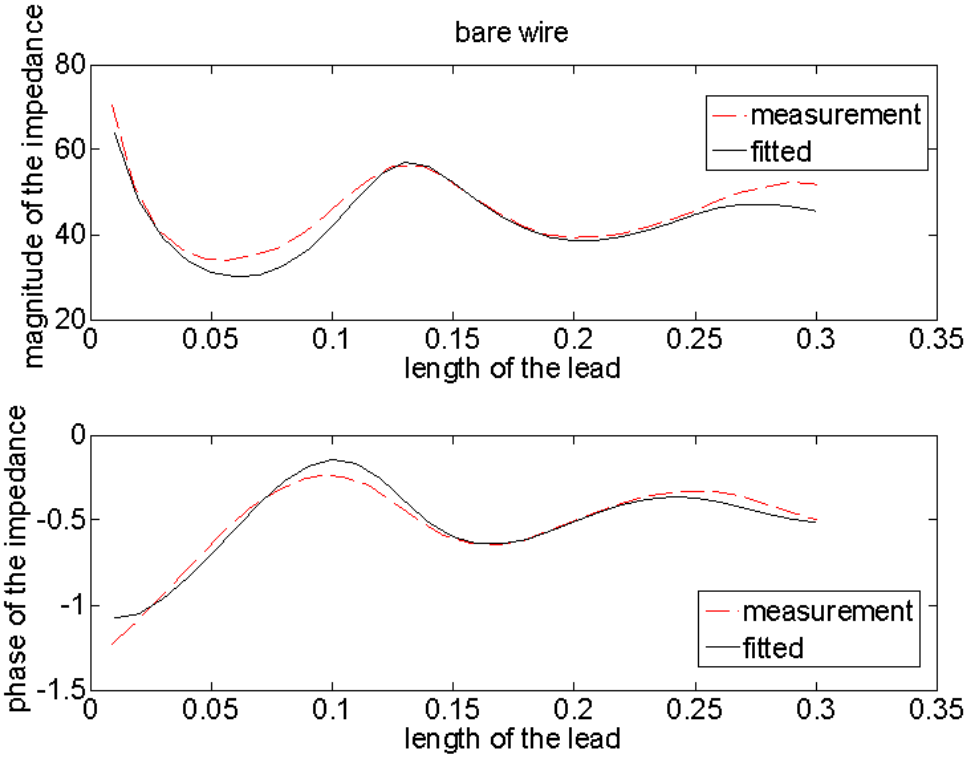

Figure 2.9: Red dashed lines are the measured impedance and the black lines are the fitting of the Equation 2.5 for bare wire.

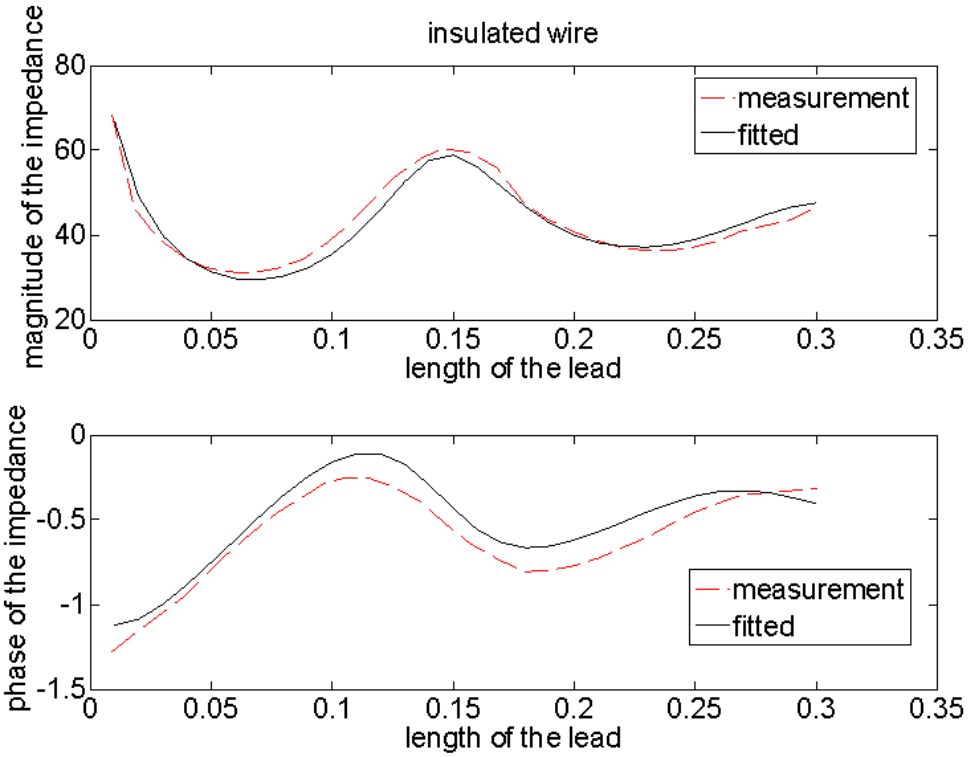

Figure 2.10: Red dashed lines are the measured impedance and the black lines are the fitting of the Equation 2.5 for insulated wire

2.5.2 Simulation Results

Circuit model parameters of the PEC box (1.2cm×4.4cm×5cm) inside the medium with relative permittivity 55 and conductivity 0.17S/m, at 123MHz, which is resonance frequency of Siemens 3T TimTrio scanner under a 1V/m incident field are found as follows: $V_c = -20.5 + j11.3$mV and $Z_c = 0.96 - j1.3\Omega$. These values are used as boundary conditions to solve the induced currents on the leads. In Figure 2.11, induced currents on the leads with lengths 40.3cm, 35.3cm, and 27.3cm are solved for with MoTLiM and compared with the MoM simulations. The blue solid lines are the MoTLiM solutions, and the red dashed lines are the MoM solutions of the induced currents. At $s = 0$, the leads are connected to the IPG case. The errors are 6.1%, 8.7% and 6.0% for the lead lengths 40.3cm, 35.3cm, and 27.3cm, respectively.

The circuit model parameters of the spherical electrode inside the medium with relative permittivity 81 and conductivity 0.42S/m, and at 123MHz under 1V/m, the incident field is found to be $V_e = -20.5 + j4.1$mV and $Z_e = 149 - j137\Omega$. Similar to the IPG case, the electrode model is used in the boundary conditions to solve for the induced currents on the leads. In Figure 2.12, induced currents on the leads with lengths 25 cm, 35cm and 35cm are solved for using the MoTLiM and compared with the MoM simulations. The blue solid lines are the MoTLiM solution, and the red dashed lines are the MoM solutions of the induced currents. The leads are connected to the electrodes at the ends where the position s has a positive value. The errors are 4.6%, 4%, and 3.3% for the lead lengths 25cm, 35cm, and 45cm, respectively.

Then, the Thevenin voltage and impedance of the bare lead with length 25cm and radius 0.1mm found as follows: $V_{th} = 8.7 - j28.6$mV and $Z_{th} = 37.7 + j4.88\Omega$. In Figure 2.13, the real power and SAR reach the maximum values, where the imaginary part of the sum of Z_{th}, Z_e and Z_m equals zero.

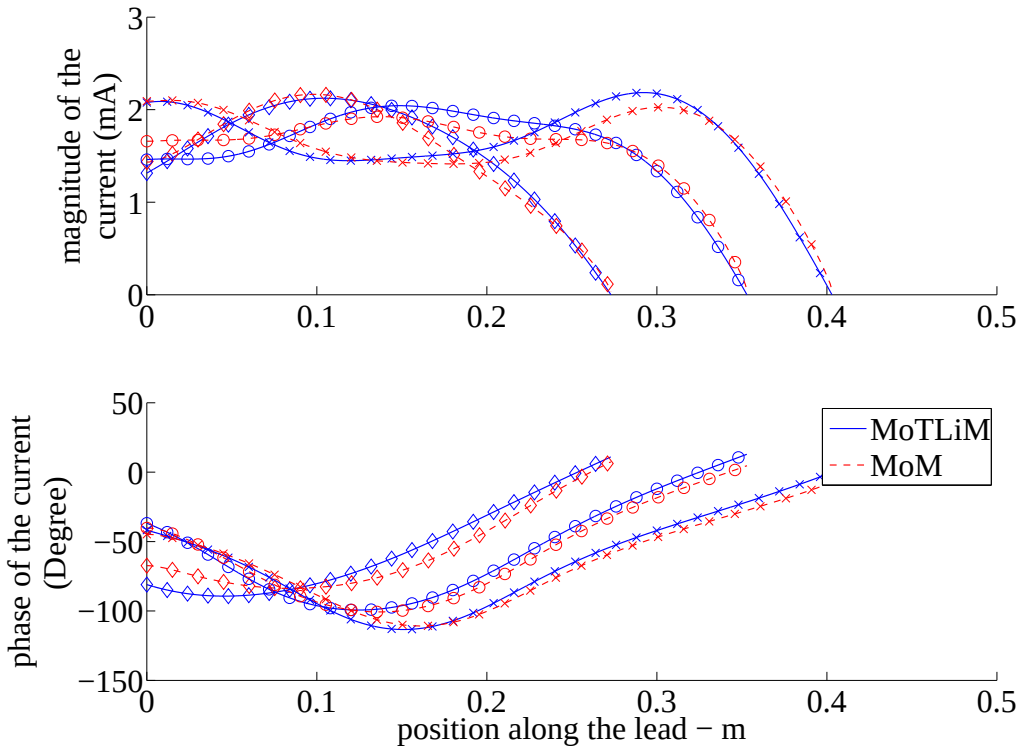

Figure 2.11: The induced currents on the leads with the IPG case connection under 1V/m uniform E-field incidence. Three bare leads with radius 1mm and lengths 40.3cm ($\times$), 35.3cm ($\circ$), and 27.3cm ($\diamond$) are connected to a PEC IPG case at the position $s = 0$. The blue solid lines are the solution obtained from the MoTLiM and IPG case model, and the red dashed lines are the MoM solution results.

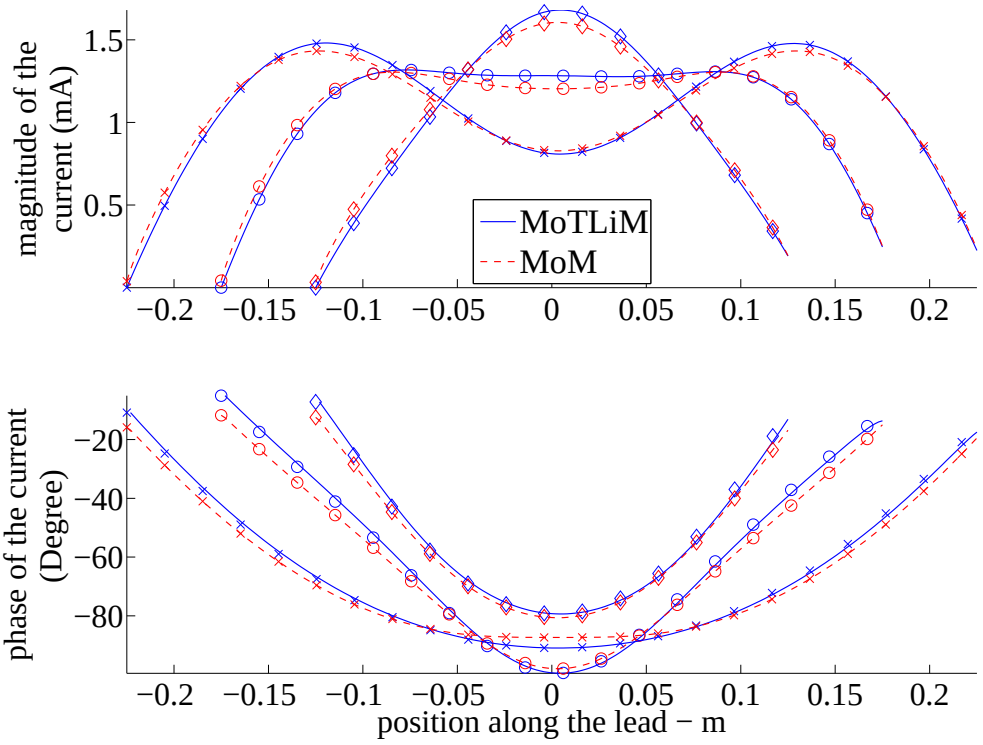

Figure 2.12: The induced currents on leads with electrode connections under 1V/m uniform E-field incidence. The blue solid lines are the solution obtained using the MoTLiM and IPG case model, and the red dashed lines are the MoM solution results. Three bare leads with radius 0.1mm and lengths 25cm ($\diamond$), 35cm ($\circ$) and 45cm ($\times$) are connected to a spherical electrode at the end where the position in the figure has a positive value.

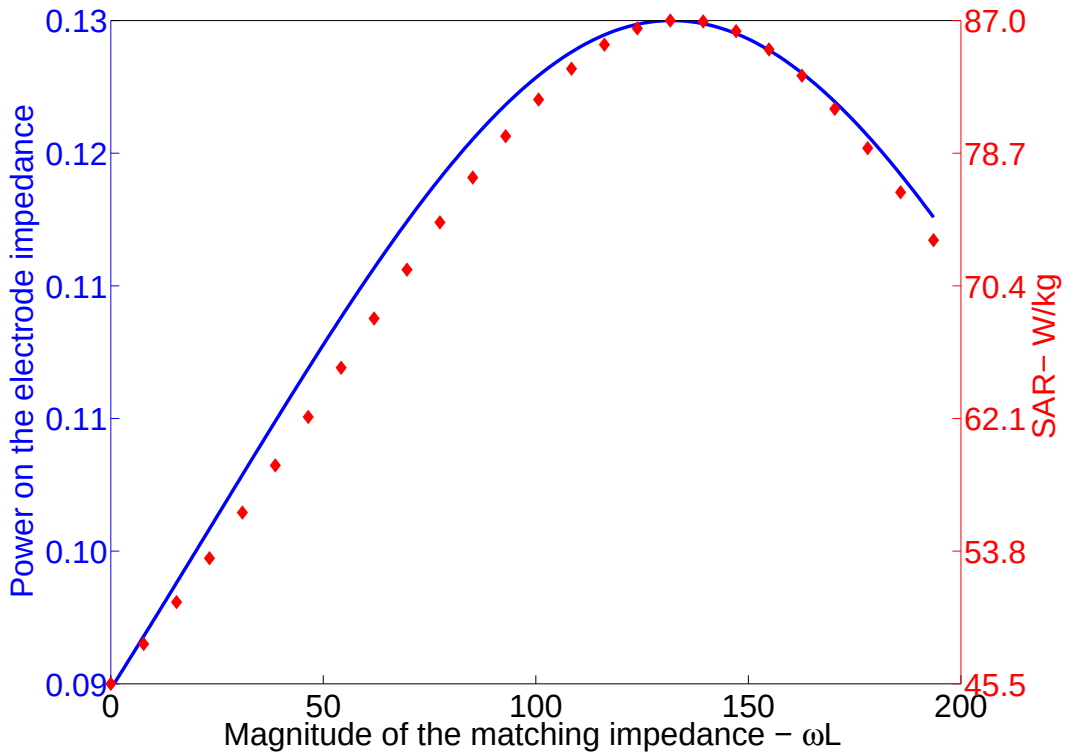

Figure 2.13: The blue solid line is the real part of the dissipated power for the impedance of the spherical electrode with radius 1mm. The red diamonds are the SAR at a point $0.1\mu m$ away from the electrode obtained using MoM simulations. The value of the matching inductance is changed from 1nH to 250nH.

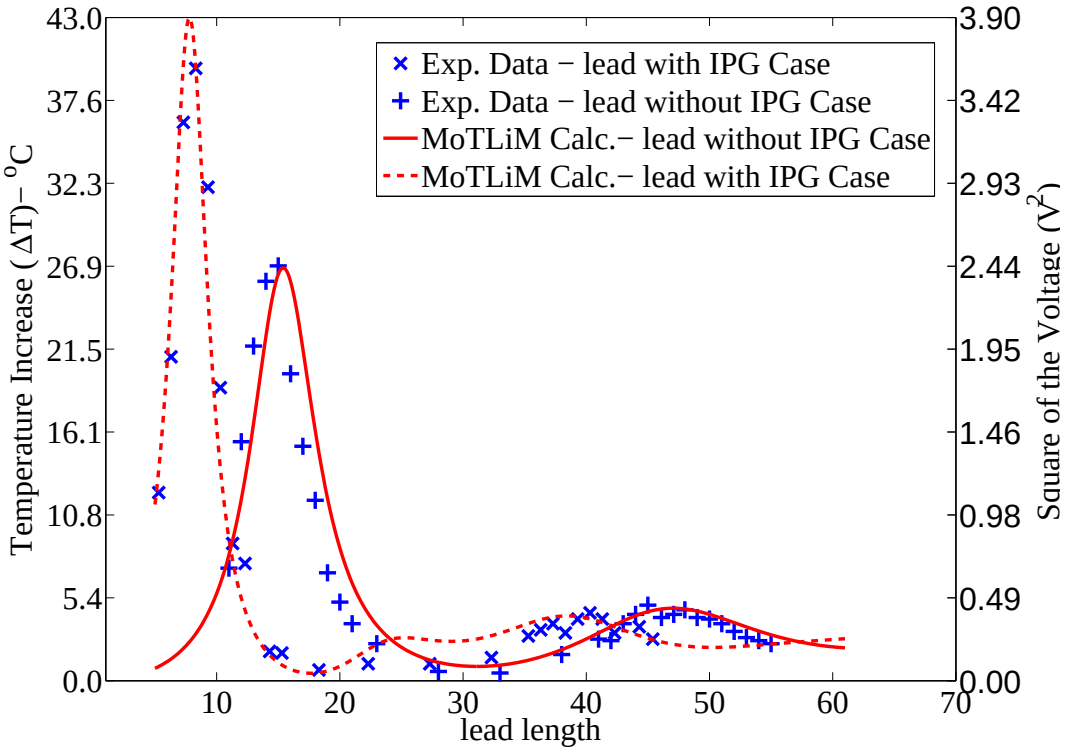

Figure 2.14: The dashed red line is the square of the hypothetical voltage at the end of the lead for different lead lengths when the lead is connected to the IPG case. The solid red line is the square of the hypothetical voltage at the end of the lead for different lead lengths. Blue $\times$ is the measured temperature rise at the lead tip when the lead is connected to the IPG case. The blue $+$ is the measured rise in the tip temperature of the lead with no connection. Left y axis is the temperature rise and right y axis is the square of the hypothetical voltage. Axis scales are adjusted for the best visualization of the trend.

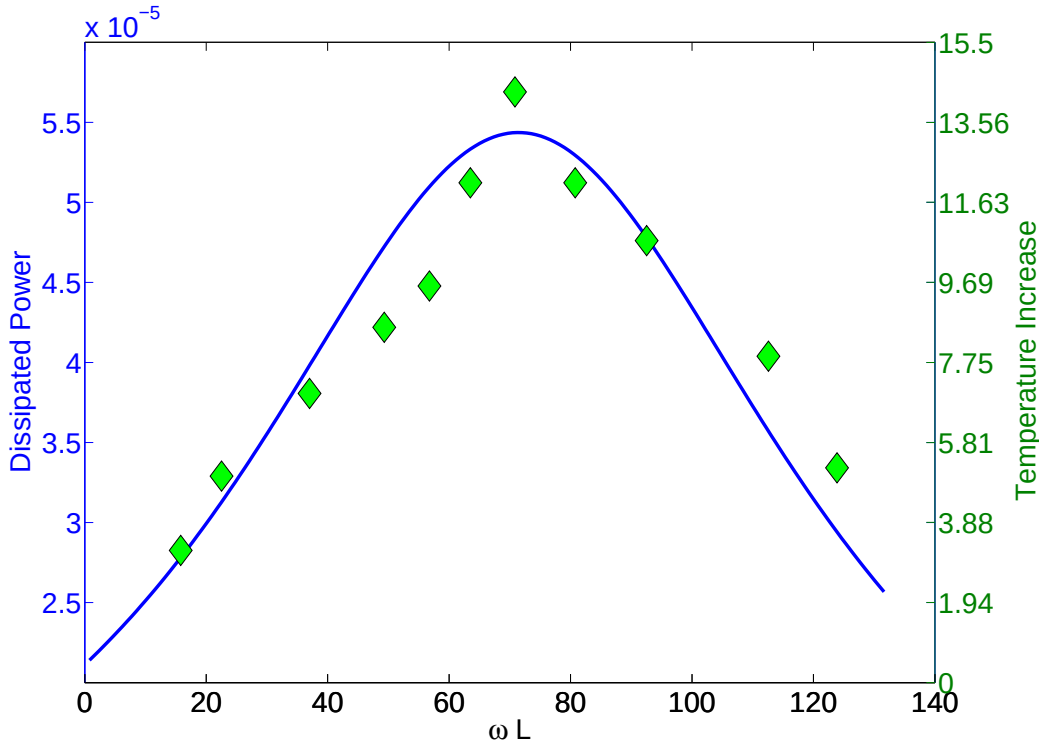

Figure 2.15: The blue solid line is the calculated dissipated power for the real part of the electrode impedance with respect to the value of the matching impedance. The green diamonds indicate the measured temperature rise with respect to the value of the matching impedance at the electrode end. Right y axis is the temperature rise and left y axis is the square of the hypothetical voltage. Axis scales are adjusted for the best visualization of the trend.

2.5.3 Experiment Results

In Figure 2.14, blue $\times$ indicates the rise in the tip temperature when the lead is connected to IPG case. The blue + indicates the rise in tip temperature when both ends of the lead are floating inside the phantom. The red dashed line indicates the square of the voltage at the tip of the lead when it is connected to the IPG case. The red solid line indicates the square of the voltage at the lead tip when both ends of the lead are floating inside the phantom. The locations of the resonance peaks are calculated with less than 13% error. The rise in tip temperature when the lead is connected to the IPG case is predicted with less than 4% error.

In Figure 2.15, the green diamonds indicate the rise in tip temperature with respect to the value of the matching impedance. The blue solid line is the calculated real power dissipated for the electrode impedance. The matching of the electrode impedance to the lead Thevenin impedance is shown, and it is also predicted using MoTLiM and the electrode circuit model. The value of the matching impedance is predicted with 0.5% error.

Chapter 3

Analysis of Guidewire with Toroidal Transceiver Antenna

Based on the similarity of currents on guidewires and transmission lines, induced currents on guidewires are solved using MoTLiM. In MoTLiM, excitation was distributed voltage sources to model the effect of incident field. When toroidal transceiver coil is used, voltage sources are zero outside of the toroidal coil and these parts can be analyzed with transmission line theory.

3.1 Currents on Guidewire with Toroidal Transceiver Antenna

In MoTLiM, conductive structures like guidewires was modeled by adding an infinitesimally small voltage source to traditional lumped element model of transmission lines as shown in Figure 3.1. These voltage sources model the effect of incident E-field on the guidewire. Also, in MoTLiM, ground is assumed to be at infinity, so the capacitance and conductance in the model are between the conductor of the guidewire and infinity. Due to the loss of the surrounding medium,

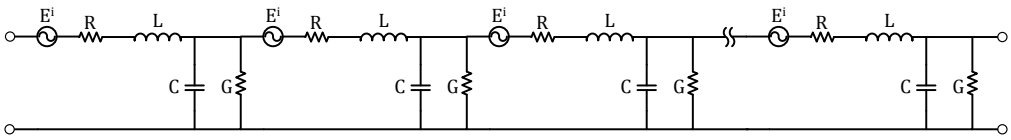

Figure 3.1: Modified transmission line model

scattered fields decay fast and lumped element parameters of the model are effected by the medium in the close proximity. Using this model the second order differential equation in Equation 3.1 can be derived as

$$I(s) + \frac{1}{k^2}\frac{d^2I(s)}{ds^2} = \frac{E^i(s)}{Z}, \tag{3.1}$$

where k is the wavenumber along the lead, Z is the distributed impedance, and s is the position along the lead. For bare and insulated guidewires detailed analysis of derivation of k and Z can be found in [12, 32].

$$\begin{aligned} Z_{bare} &= \frac{\eta k}{4} H_0^{(2)}(ka) \\ k_{t,bare} &= k \\ Z_{insulated} &= k\frac{(\eta H_0^{(2)}(kb) - \eta_d k_d b H_1^{(2)}(kb) ln(a/b))}{4} \\ k_{t,insulated} &= k\sqrt{\frac{k_d^2(H_0^{(2)}(kb) - kbln(a/b)H_1^{(2)}(kb))}{k_d^2 H_0^{(2)}(kb) - k^3 bln(a/b)H_1^{(2)}(kb)}}, \end{aligned} \tag{3.2}$$

where k and k_d are the wavenumber inside the medium and insulation, respectively, a is the radius of the conductor, b is the total radius of the guidewire with insulation, η and η_d are the wave impedance in the medium and in the insulation; respectively.

When k and Z are determined for a guidewire, Equation. 3.1 can be used to solve the current along the guidewire for a known tangential Electric Field (E-field). However, when a guidewire is used with toroidal transceiver coil and is inserted inside the body, a system shown in Figure 3.2 is formed.

For the analysis of the guidewire inside the body; MoTLiM can be used. For the case in which the guidewire is excited with the toroidal transceiver antenna; incident E-field is zero, so the MoTLiM turns into the traditional transmission line model with the parameters in Equation 3.2.

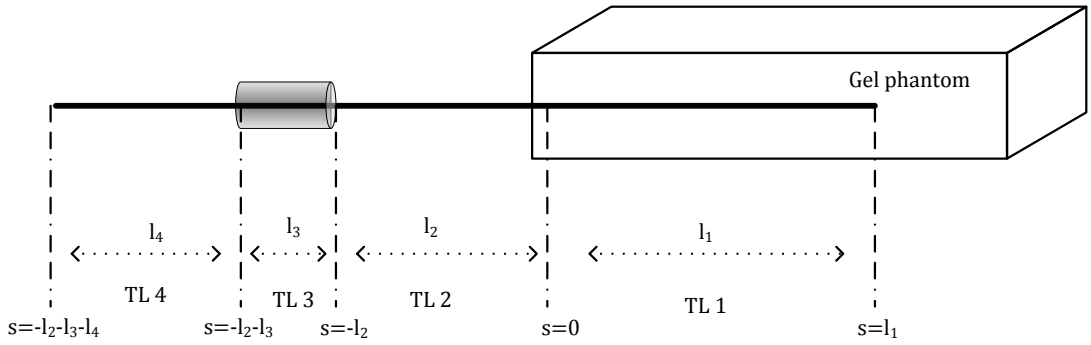

Figure 3.2: Schematic of guidewire with toroidal transceiver coil.

When incident E-field is zero, by solving Equation 3.1, current can be found as

$$I(s) = Ae^{-jk_t s} + Be^{jk_t s}, \tag{3.3}$$

Also, hypothetical voltage along the guidewire can be defined using the differential equation

$$V(s) = \frac{Z}{k^2}\frac{dI(s)}{ds}, \tag{3.4}$$

Solving the Equation. 3.4 for uniform E-field and zero incident E-field cases; hypothetical voltage can be found as

$$V(s) = \frac{-jZ}{k}(Ae^{-jks} - Be^{jks}). \tag{3.5}$$

Using the equation of continuity and Equation. 3.4 it can be shown that the hypothetical voltage is the scaled version of the charge distribution. The hypothetical voltage is helpful for defining some concepts and boundary conditions throughout the study.

To analyze the behavior of the currents on the guidewire inside the body a unit current is assumed on the guidewire at the point where the guidewire enters into the body. Then, to find unknowns A and B for each transmission line section, following boundary conditions must be applied: Current is zero at distal end of the guidewire, and if there is a transmission line boundary, i.e. guidewire is stripped, current and voltage are continuous at the boundary of transmission line sections.

3.1.1 Impedance Analysis with Smith chart

When there is E-field incidence to the guidewire, there are distributed sources along the guidewire, so transmission line equations and Smith chart can not be used without modification. However, when the source is at the end of the guidewire; Smith chart can be used for the analysis of the guidewire. To use the Smith chart complex characteristic impedance of guidewire must be found. In transmission line theory, characteristic impedance is defined as the ratio of voltage wave to current wave traveling in the same direction. So characteristic impedance can be defined as follows;

$$Z_{cn} = \frac{-j(Z_n/k_n)A_n e^{-jk_n s}}{A_n e^{-jk_n s}} = \frac{-jZ_n}{k_n}. \tag{3.6}$$

As characteristic impedances for each section is defined, impedance can be found at any point along the guidewire using impedance formula of lossy transmission line, i.e.,

$$Z = Z_{cn}\frac{Z_l + Z_{cn}\tanh(jks)}{Z_{cn} + Z_l\tanh(jks)} \tag{3.7}$$

or using a Smith chart.

3.1.2 Effect of Stripping the Tip of the Guidewire

In Etezadi-Amoli et al.'s work; it is shown that stripping the tip of the guidewire increases the B_1 intensity at the tip of the guidewire. Here this effect is analyzed using the proposed method. Using a guidewire with radius 0.6mm and insulation thickness 0.5mm; induced currents on the guidewire is solved when guidewire is inserted inside the medium with electrical conductivity of 0.5S/m and relative permittivity of 88. Relative permittivity of insulation is 4 and conductivity of the insulation is 0. Length of the guidewire inside the medium is kept 40cm and length of the stripped part is changed between 0.01cm and 36cm. For this analysis both insulated and bare parts of the guidewire is treated as transmission lines. Then, B_1 field along the guidewire is found using the Biot-Savart law.

Then the impedance at the point where the guidewire is inserted to the body

is calculated for insulated guidewires. Radius of the guidewires are changed from 0.1mm to 1mm while the insulation thickness is kept as 0.1mm. Relative permittivity and conductivity of the insulation is 4 and 0, respectively. Length of the guidewire is 55cm with 1cm stripped tip. These calculations are done inside the medium with electrical conductivity 0.5S/m and relative permittivity 88. Then, B_1 field along the guidewire is found using EM simulations using FEKO.

3.2 Results

Figure 3.3 depicts the magnitude of the B_1 field at the point 1cm far from the guidewire tip and 0.1mm radially far from the guidewire when the tip of the guidewire is stripped from 0.1mm to 36cm. Total length of the guidewire is 40cm, guidewire radius is 0.6mm and insulation is 0.5mm. Calculations are carried out inside the medium with electrical conductivity of 0.5S/m and relative permittivity of 88 which are the electrical properties that are used by Etezadi-Amoli et al. and operating frequency is 64MHz. Relative permittivity of the insulation is 4 and electrical conductivity is 0. Wavenumber of the bare guidewire is calculated as $25.92 - 9.37j$, and characteristic impedance is $24.58 + 1.59j$. Wavenumber of the insulated guidewire is calculated as $12.42 - 2.17j$, and characteristic impedance is $53.49 - 5.56j$.

In Figure 3.4; characteristic impedance and wavenumber of the insulated and bare guidewires are shown at 123MHz. Radius of the guidewire is varied from 0.1mm to 1mm while the insulation thickness is kept as 0.1mm. Total length of the guidewire is 55cm and tip of the guidewire is stripped for 1cm. In Figure 3.5 impedance along the guidewire is shown. Note that each guidewire has different radius hence different characteristic impedances. To be able to plot them on the same Smith chart impedances are normalized to the 50Ω. In Figure 3.6 B_1 maps which are obtained from FEKO simulations along the guidewire are shown. FEKO simulations are conducted by applying current source to the last segment of the guidewire. However, for different radius guidewires; applied current changes

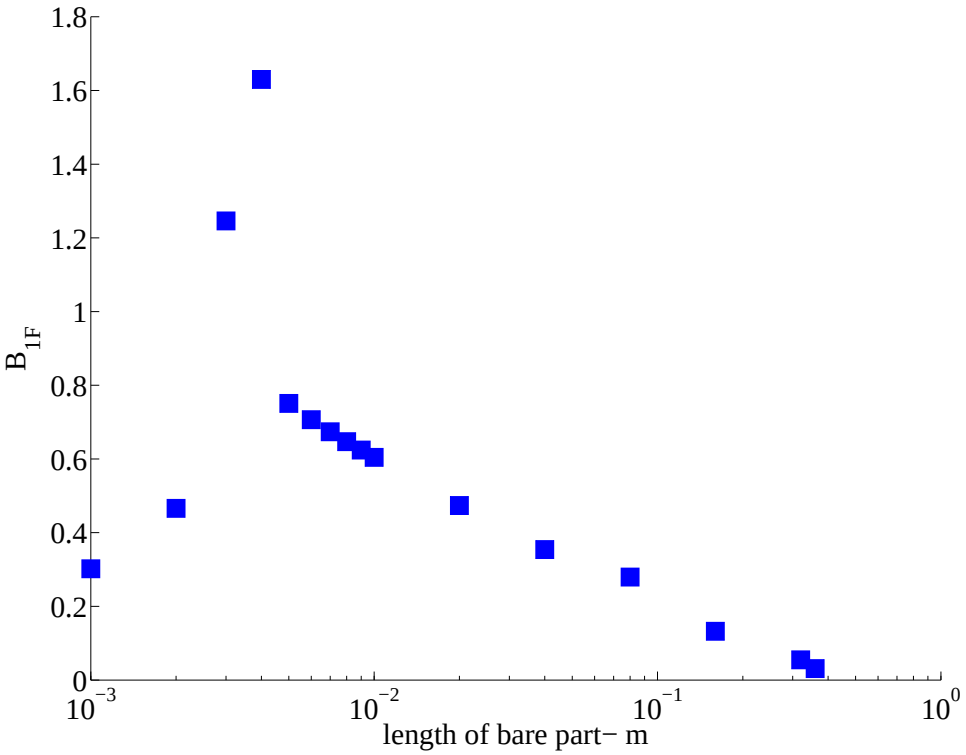

Figure 3.3: B_1 values at the tip of the insulated guidewire with bare tip. Tip of the guidewire is striped for lengths from 0 to 36cm. Guidewire radius is 0.6mm in insulated case, insulation thickness is 0.5mm, and relative permittivity is 4.

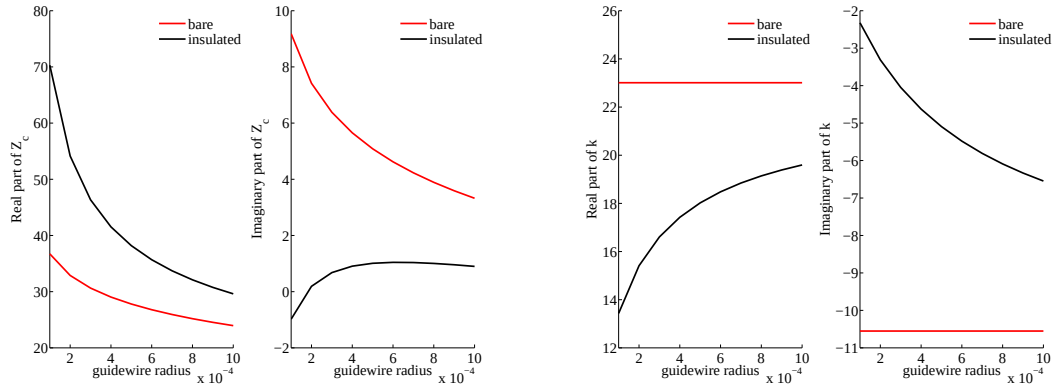

(a) (b)

Figure 3.4: Real and imaginary part of respectively the characteristic impedance and the wavenumber of the insulated and bare guidewire sections when radius of the guidewire is changed from 0.1mm to 1mm while the insulation thickness is kept 0.1mm.

as the impedance seen by the source is changed. So for compression, B_1 fields are normalized to the magnitude of maximum value of each simulation result.

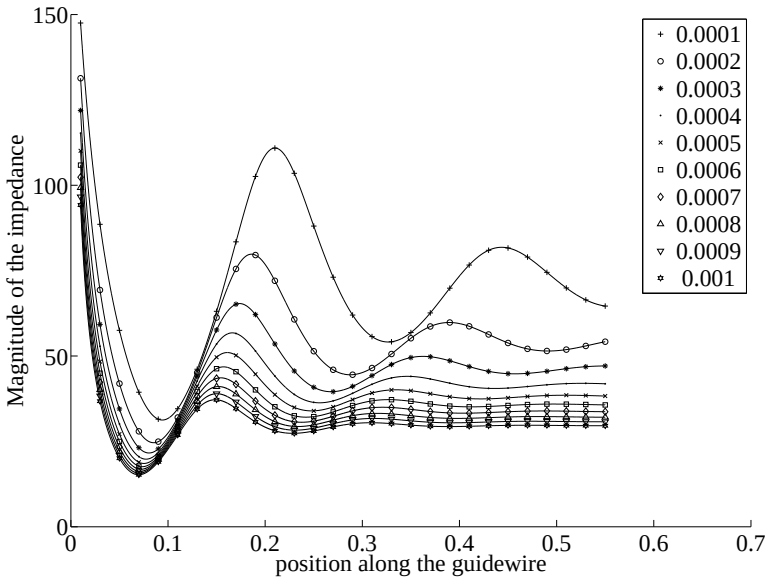

(a)

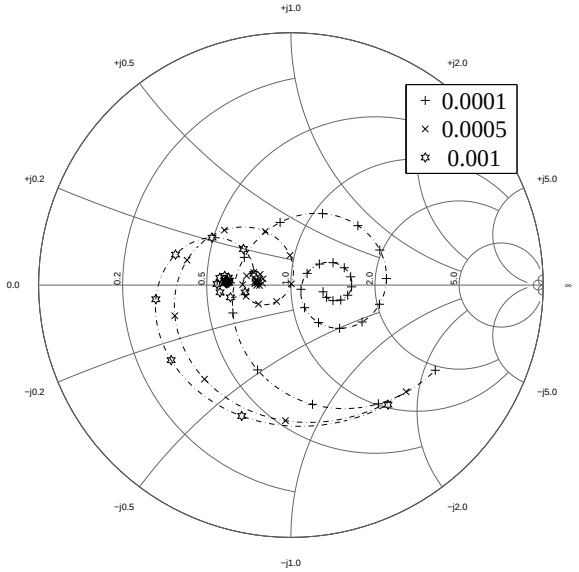

(b)

Figure 3.5: Impedance along the guidewire starting from the tip and moving to the point where the guidewire inserted into the body, for guidewire radius from 0.1mm to 1mm while the insulation is kept as 0.1mm. (b) is the impedance along the guidewire plotted on the Smith chart. Note that each guidewire has different radius hence different characteristic impedances. To be able to plot them on the same Smith chart; impedances are normalized to 50Ω

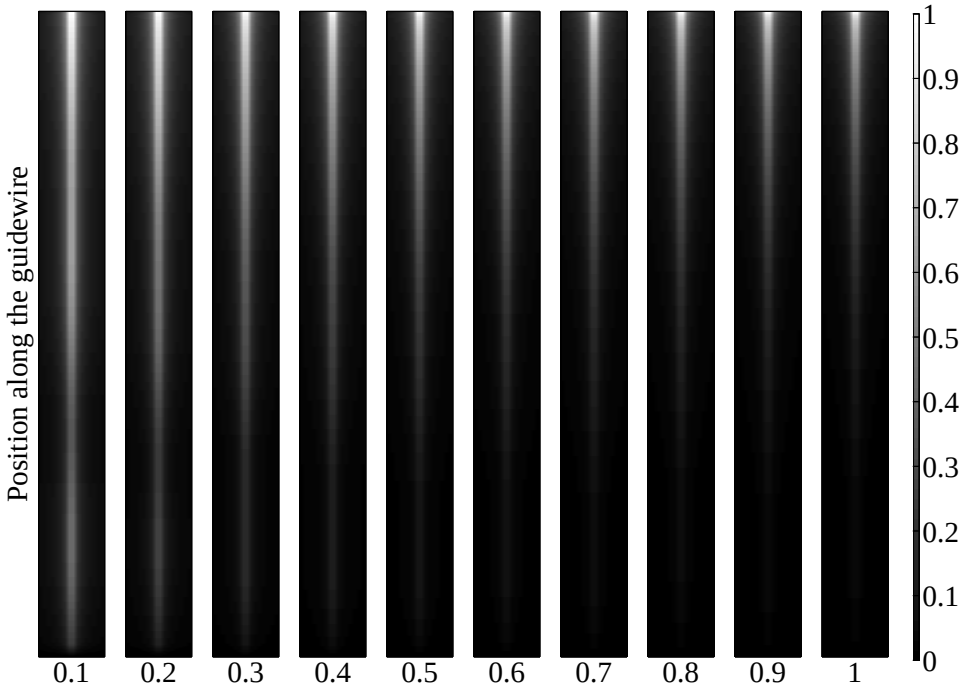

Figure 3.6: Magnitude of the B_1 fields along the guidewire.

Chapter 4

MRI Based Electrical Properties Measurement Techniques

In this part, an MRI based electrical properties measurement technique is presented for the verification of the coaxial transmission line fixture for electrical properties measurement, which was presented by Akin et al [28]. The MRI based method is developed using MoTLiM [12] and the tip temperature increase of wires during an MRI scan. This method is capable of measuring electrical properties of substances without convection. Coaxial transmission line (CTL) fixture is capable of measuring fluid substances. For the comparison of the results obtained by both methods, Hydrocyethyl cellulose (HEC) phantoms are used. HEC phantoms are in gel form so that they can be filled into the CTL fixture and have no convection so that they can be used for MRI temperature increase experiments. The comparison of these two methods are done to gain confidence in measurements.

4.1 Theory

4.1.1 MRI Based Method

As explained in previous chapters, in MoTLiM, induced currents along the wire inside a lossy tissue is defined with a differential equation as follows;

$$I(s) + \frac{1}{k_t^2}\frac{d^2I(s)}{ds^2} = \frac{E^i(s)}{Z} \tag{4.1}$$

where Z impedance per unit length, k_t effective wavenumber along the wire, s is the position along the wire and $E^i(s)$ is the tangential the incident E-field. When a bare perfect conductor is considered the effective wavenumber is equal to wavenumber of the surrounding medium [12] ($k_t = \omega\sqrt{\mu\epsilon - i\sigma/\omega}$) and contains all information about the permittivity and conductivity of the medium. Also using the lumped element model, voltage along the wire can be defined as follows;

$$V(s) = \frac{Z}{k^2}\frac{dI(s)}{ds} \tag{4.2}$$

The voltage along the wire can be used for the calculation of the power deposited to the phantom as

$$I(s) = Ae^{-jk_ts} + Be^{jk_ts} + \frac{E_0}{Z} \tag{4.3}$$

$$V(s) = \frac{-jZ}{k_t}(Ae^{-jk_ts} - Be^{jk_ts}), \tag{4.4}$$

In both equations, unknowns A and B can be found by applying boundary conditions. For a wire with both ends are floating inside the tissue, boundary conditions can be applied as

$$\begin{aligned} I(s = -l_w/2) &= 0 \\ I(s = l_w/2) &= 0, \end{aligned} \tag{4.5}$$

where l_w is the length of the wire. Using these boundary conditions current and voltage along the wire can be found as

$$\begin{aligned} I(s) &= \frac{E_0}{Z} - 2\frac{E_0}{Z}\frac{\sin(k_t\frac{l_w}{2})}{\sin(k_tl_w)}\cos(k_ts) \\ V(s) &= 2\frac{E_0}{k_t}\frac{\sin(k_t\frac{l_w}{2})}{\sin(k_tl_w)}\sin(k_ts). \end{aligned} \tag{4.6}$$

Assuming that the loss of the medium is high such that the scattered fields decay fast, the temperature increase at the tip can be related to the power at the tip of the wire. Therefore, temperature increase at the tip can be written as

$$\Delta T = C|\frac{2E_0}{k_t}\tan(k_t l_w/2)|^2, \tag{4.7}$$

where C is the constant, showing operations to find SAR and temperature increase. Relationship between charge density and SAR is a linear operation. Similarly, the relationship between SAR and temperature increase can be found using alternative techniques [33, 34], which are also linear approximations.

ΔT depends on the thermal conductivity of the substance under test and exposure time. When a bare wire is used, $k_t = \omega\sqrt{\mu\epsilon - i\sigma/\omega}$ and fitting Equation 4.7 to the measured temperature rise for k_t gives the electrical conductivity and permittivity of the surrounding medium.

4.1.2 Coaxial Transmission Line (CTL) Based Method

As shown in Figure 4.1, when SUT is placed inside the fixture, a system of serially connected coaxial lines is obtained. First part is the air filled coaxial line, second is the SUT filled coaxial line, and last part is polyoxymethylene filled coaxial line. During measurements, end of the air filled part remains open and impedance at the polyoxymethylene end is measured. The impedance at the polyoxymethylene end can also be calculated using transmission line theory [35]. In well known transmission line theory, impedance at a distance l from the load can be found as

$$Z(l) = Z_0\frac{Z_L + Z_0\tanh(\gamma l)}{Z_0 + Z_L\tanh(\gamma l)}, \tag{4.8}$$

where Z_0 is the characteristic impedance of the transmission line, γ is the propagation constant of the transmission line, and Z_L is the termination load. Assuming that the conductor loss is zero, Z_0 and γ of a coaxial transmission line can be

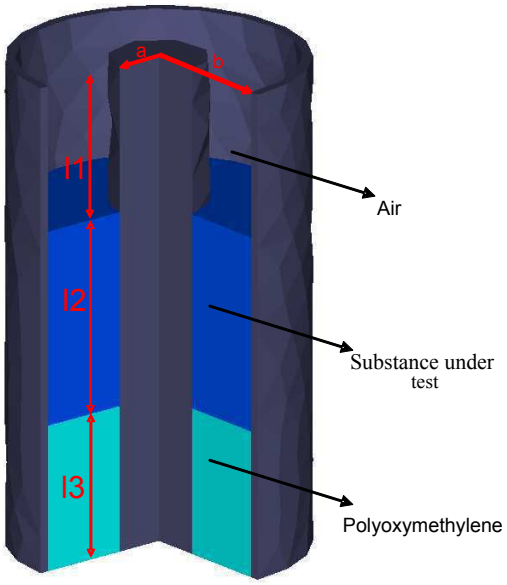

Figure 4.1: Fixture geometry. a and b are the radius of inner and outer conductors, respectively. Bottom of the fixture is polyoxymethylene substrate. Second part is filled with the substance under test and the remaining part is air.

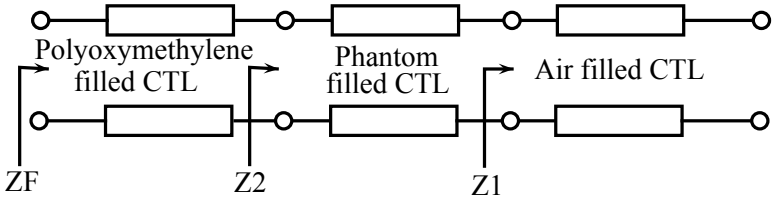

Figure 4.2: Circuit model of CTL fixture. When the SUT is filled inside the fixture it forms three serially connected transmission line system.

written as

$$\begin{aligned} Z_0 &= \frac{ln(b/a)}{2\pi}\sqrt{\frac{j\mu}{\epsilon'' + j\epsilon'}} \\ \gamma &= \omega\sqrt{j\mu\epsilon'' - \mu\epsilon'}. \end{aligned} \tag{4.9}$$

Also the loss of the air and polyoxymethylene can be negligible. For the presented fixture impedance at the polyoxymethylene end can be found by calculating impedances at each step as shown in Figure 4.2. By using Equation 4.8 ZF, can be found in three steps: First using open circuit as Z_l and TL parameters for air $Z1$ can be found, second using $Z1$ as Z_l and TL parameters for SUT, $Z2$ can be found and third using $Z2$ as Z_l and TL parameters for polyoxymethylene

ZF can be found.

4.2 Methods

For the comparison of two proposed methods, HEC, NaCl and water solutions are used. Three different substances are prepared using 14g HEC per liter water and NaCl concentration is 0g, 0.5g, 1g per liter water. These electrical properties substances are measured using both proposed method.

As the MRI experiment method depends on the temperature increase it is important to know the behavior of the electrical properties with the change in temperature. So the electrical properties of the deionized water is measured by changing the temperature of the water from 8° Celsius to 63° Celsius. As the phantoms that are used during experiments are water based it is good assumption to expect the behavior of phantom is similar to behavior of water.

Furthermore, using the CTL fixture, change in the electrical properties with respect to frequency between 60MHz and 140 MHz, is measured for water NaCl solutions with concentrations between 1g/L and 6g/L and compared with the literature. Also electrical properties of blood samples are measured with CTL fixture and compared with the literature.

4.2.1 Measuring Electrical Properties with MRI Experiments

During the tip heating experiments a bare copper wire with diameter 0.5mm is placed inside a cylindric HEC phantom on a co-centered circular path at the middle of the height of the cylinder. The cylindric phantom is placed inside a birdcage transmit coil as the phantom and birdcage coil become co-centered. By this geometry uniform tangential E-field incidence is guaranteed on the wire. For these experiments HEC phantoms with concentration of 14g HEC per liter water

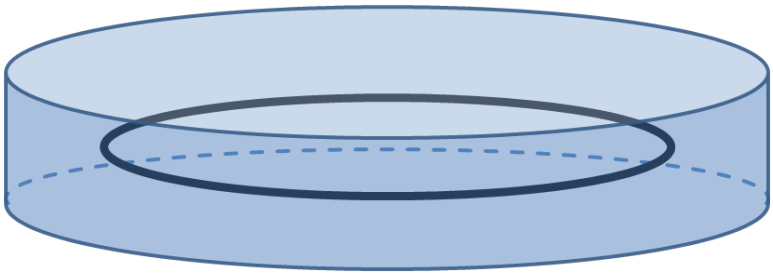

Figure 4.3: Experimental setup for MR experiments. A cylindrical phantom is built and filled with substance under test. Wire is placed on a circular path, shown as black line in the figure, and co-centered with the phantom

and 0g, 0.5g, 1g NaCl per liter water are used For heating experiments TRUFI sequence is used with parameters, which are adjusted to reach maximum allowable SAR from the scanner, TR= 3.79ms and FA= 81. Temperature increase at the lead tip is measured with fiberoptic temperature probes (Optical Temperature Sensor, Neoptix Reflex-4 RFX134A) for wire lengths varying between 7cm and 60cm. Then Equation 4.7 is fitted to the measured temperature increase to find the conductivity and permittivity of the phantom material. For fitting, non-linear least squares method is used.

4.2.2 Measuring Electrical Properties with CTL Fixture

Permittivity and conductivity measurements are done using the fixture with 3mm inner radius and 11.15mm outer radius. Impedance measurements are performed with Agilent E5061A series network analyzer as shown in Figure 4.4. The fixture is connected to the network analyzer with a coaxial cable (Huber+Suhner K_02252_D-08). 1-port calibration is done at the fixture end of the coaxial cable. Also effect of the BNC connector on the fixture is taken into account. First, for an empty fixture($l_2 = 0$), the impedance that must be measured is calculated then using port extension measurement for empty fixture is corrected. Then, calibration process fixture is filled with phantom, and measurements are carried out for several l_2 values. For each measurement l_2 value is also measured. Then using Equation 4.8, reflection coefficient at the polyoxymethylene end of the CTL fixture is calculated. An error is defined between measured and calculated reflection

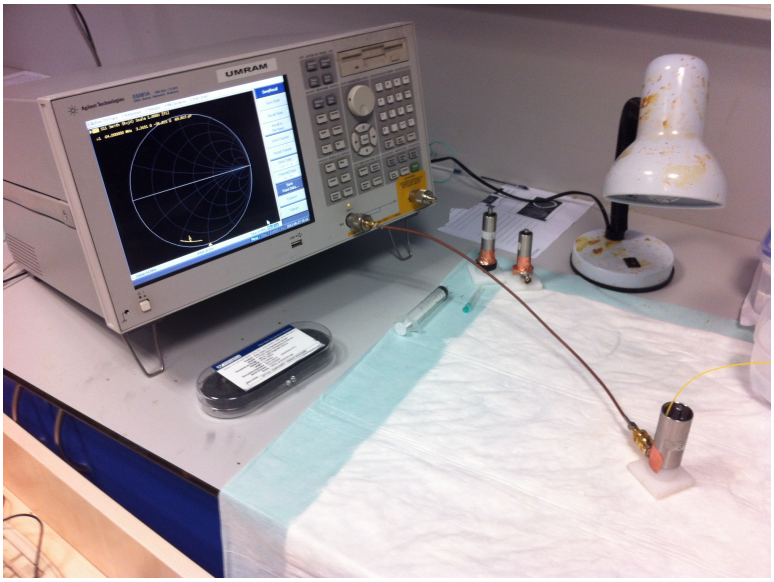

Figure 4.4: Experimental setup for CTL fixture measurements. CTL fixture is connected to a network analyzer using a coaxial cable. Calibration is done at the cable-CTL connection point.

coefficient as

$$error = |\Gamma_{measured} - \Gamma_{calculated}|. \tag{4.10}$$

The reflection coefficient is calculated by changing the conductivity and permittivity of the substance until the error becomes less than 10^{-12}. This error minimization is done for every value of l_2 and a linear fit is done to the calculations to find conductivity and permittivity.

4.3 Results

In Figure 4.5, temperature increase at the tip of the wire with respect to wire length and the fit of the Equation 4.7 are shown.

Conductivity and permittivity of different gel solutions (contents are shown in Table 4.1) are measured by using both proposed methods and compared. In Table 4.1, measured conductivity and permittivity of three different phantoms with two different methods are shown. As a measure of accuracy, an error is

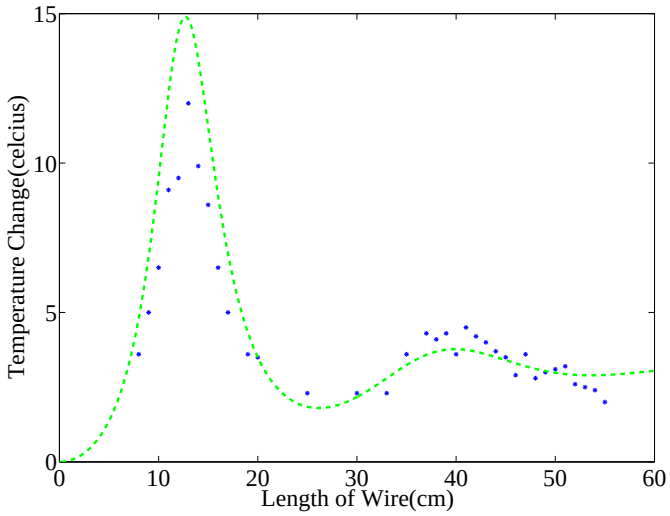

Figure 4.5: Fitting of Equation 4.7 to the measured temperature increase during the MR experiment. The phantom is solution of 14g HEC/L and 0.5g NaCl/L water.

Solution	Measured with CTL ($\sigma_{ctl}, \epsilon_{r,ctl}$)	Measured with MRI experiments ($\sigma_{MR}, \epsilon_{r,MR}$)	Difference (σ, ϵ)
14g HEC/L	0.14S/m, 66	0.19S/m, 65.8	27.9% , 0.23%
14g HEC/L 0.5g NaCl/L	0.26S/m, 60	0.35S/m, 70.1	1.52% , 11.8%
14g HEC/L 1g NaCl/L	0.36S/m, 58	0.46S/m, 51.8	2.79% , 8.73%

Table 4.1: Solution contents and their conductivity and permittivity values that are measured with CTL fixture and MRI experiments. The last row is the difference between two measurement methods calculated as in Equation 4.11

defined between two different measurement techniques as

$$\begin{aligned} \sigma_{error} &= \frac{|\sigma_{MR} - \sigma_{ctl}|}{\sigma_{MR}} \\ \epsilon_{error} &= \frac{|\epsilon_{MR} - \epsilon_{ctl}|}{\epsilon_{MR}}, \end{aligned} \tag{4.11}$$

where subscript MR is the measurements that are done using MoTLiM formulation and MRI experiments and ctl is the measurements that are done with CTL fixture. The differences between estimated permittivity values are below 5% and the difference of conductivity values are below 34%.

Chapter 5

Discussion and Conclusion

In this work, the electrode and case parts of an active implantable device (IPG) are modeled with an electrical circuit at operating frequency of 3T scanner, which is the available on site. A novel method is developed to find the parameter values of the circuit model at RF frequency. The electrical circuit model contains an impedance and a voltage source. The impedance models the interaction of the electrode/IPG case with the tissue, and the voltage source shows the effect of the incident field. To find the parameter values, both MoTLiM and MoM simulations are used. Reason of using MoM is its capability of solving currents on wire, however any other numerical method could also be used. The values of the circuit model parameters determined are tested using MoM simulations and MRI experiments. A uniform E-field incidence is used for all of the derivations, simulations, and experiments for the sake of simplicity. All concepts can be re-derived using the methods explained here for a known E-field incidence. It is shown that MoTLiM [12] is capable of solving currents for nonuniform E-field as long as the tangential component of the E-field is known. If the E-field variation on the electrode and IPG case is small compared to wavelength, it can be neglected. However, if the E-field variation on the electrode and the IPG case is high, then circuit parameters must be found using the presented method.

It is also highly possible that the AIMD lay inside different tissues. Because

defined IPG case and electrode impedances are medium dependent, they must be found using the electrical properties of the medium which the IPG case and electrode are surrounded. Also, lead could be passing through different tissues. For this situation lead can be considered as serially connected transmission lines with different k_t and Z values.

The theory of MoTLiM is extended with the circuit models of the IPG case and the electrode parts of an AIMD. Using MoTLiM, the lead part is analyzed, and with the proposed circuit models, the effects of the IPG case, electrode, and any lumped circuit element placed between these parts could be analyzed. With this theory, a complex scattering problem is recast as a circuit problem, and any modification could be solved easily.

To test the IPG case, induced currents are calculated using the MoTLiM, and the circuit model is then compared with the MoM simulations. The error in the solutions is below 10%. Then, the IPG case model is tested using the MRI experiments. The square of the hypothetical voltage is calculated at the end of the lead, with the IPG case connection at the other end. The square of the hypothetical voltage is also found for the lead without a connection to any IPG case or electrode. Then, MRI experiments are conducted for these cases. A bare lead is connected to a PEC box and placed inside a uniform phantom. The tip heating is then measured by changing the lead length. The tip temperature rise is measured for the same lead with no case connection. These data are then compared with the calculations. The locations of the resonance peaks are predicted with and without the IPG case with a less than 13% error. The change in the magnitude of the temperature rise when the IPG case is connected to the lead is predicted with a less than 4% error.

To test the electrode, induced currents on the leads are solved for different lead lengths. The MoTLiM results are compared with the MoM simulations. The error in the induced currents is less then 5%. Then, the power matching concept is demonstrated with simulations and experiments. A matching inductor is placed between the electrode and the lead, and the power dissipated for the real part of the electrode impedance is calculated by changing the inductance

value. When the electrode impedance is matched to the lead Thevenin impedance, the dissipated power for the real part of the electrode impedance reaches its maximum. MRI experiments are conducted for the same scenario. It is shown that at the matching condition, the temperature rise at the electrode reaches its maximum. This result is important, as replacing the inductor between lead and electrode is used for preventing a temperature rise at the electrode end [36]. However, it is shown that the value of the inductance must be chosen carefully, as it can affect the tip temperature rise.

The analysis is conducted to determine the square of the hypothetical voltage. In the quasi-static region, the scattered fields decays fast due to the loss of the medium, the square of the hypothetical voltage at the tip of the lead had a linear relationship with the SAR, and the temperature rise is calculated using linear approximations [5, 37] from the SAR distribution. In the case these assumptions fail, the SAR can be solved for using the whole hypothetical voltage distribution along the lead.

With the presented data it is shown that IPG case and electrode can be modeled with a simple circuit model. Although all modeling is done for 3T, which is available on site, all derivations can easily be done for 1.5T as frequency is just a parameter in k_t and Z [12]. Presented circuit models can be helpful in order to choose correct IPG case, lead and electrode combinations. In the literature, there are studies [10] which show that using a lead with different electrodes will result in different temperature rise in the tissue, and these studies are mostly based on experimental methods. After defining the electrode and lead Thevenin impedances, results of these experiments can be interpreted as mismatch between these impedances. In this work it is shown that by matching the electrode impedance to the lead Thevenin impedance temperature rise can be maximized. This fact can also be used adversely and impedances can be chosen as the current flowing through the electrode is small such that it does not cause excessive heating.

In the IPG case experiments, it is shown that the presence of the IPG case drastically changes the resonance length and the amount of temperature rise.

With the IPG case circuit model this length can be predicted with less than 13% error. So this fact can be useful for avoiding resonance.

Also, these models are useful tools for the implant tests. An AIMD is modeled with six parameters (two for each part). Once these parameters are known worst case scenarios can be predicted. In addition, effect of modifications on the lead can be examined. Weiss et al. [14, 38] proposed MRI safe transmission line using transformers and matching networks to connect transmission line sections. Their design can be easily analyzed with MoTLiM models. Inductance, resistance and stray capacitance of transformer sections and matching networks can easily be integrated into MoTLiM and can be analyzed. Optimization of the device can easily be done with MoTLiM modeling. Ladd et al. [39] proposed placing RF chokes on the leads. Effect of these chokes can also be analyzed with MoTLiM modeling. Resistance of these chokes can be integrated on the MoTLiM model and interaction with electrodes and IPG cases can be analyzed.

Furthermore, in this study guidewire with toroidal transceiver antenna is analyzed using the MoTLiM. Currents on the guidewire is solved when it is excited by the toroidal transceiver coil and using the current on the guidewire B_1 distribution around the guidewire inside the body is solved insulated and stripped tip guidewires. It is shown that insulation increases the signal intensity around the guidewire. Also, signal intensity at the tip can be increased with stripping the tip. When guidewire is stripped there is a increase in the signal intensity at the boundary of striped and insulated sections. As striped length increases tip visibility converges to bare wires tip visibility. This phenomena can be used as marker to show the tip of the guidewire.

Additionally, impedance analysis on the guidewire is done with Smith chart. Note that the impedance is between guidewire and the ground which is assumed to be at the infinity. Also, the impedance is the result of the standing wave pattern of current on the wire. However, due to the loss of the body, impedance on the guidewire inside the body follows a spiral path on the smith chart and converges to the characteristic impedance of the guidewire. This behavior is the result of dissipation of power along the guidewire and when the impedance reaches

to the characteristic impedance current on the guidewire decays to zero before it reaches to the tip of the guidewire. In this case tip visibility of the guidewire is lost.

Furthermore, MoTLiM is used for verification of the coaxial transmission line fixture for electrical property measurement of phantom materials. The temperature increase at the wire tip is formulated (Equation 4.7) using MoTLiM and used for measurement of electrical properties of phantoms. In the Equation 4.7 permittivity dominates the location of the resonance peaks whereas conductivity determines the sharpness (Q) of the resonance peaks. So as the Q of the resonance peaks are more sensitive to the errors in temperature increase measurements, misalignment of the optical probe can easily leads to higher errors while predicting the conductivity of the phantom. Although MRI based method depends on the temperature increase, the change in electrical properties with temperature does not have significant effect on the MRI based method. The only significant temperature increase occurs at the tip of the wire but the formulation of the proposed MRI based method uses the permittivity and conductivity of whole medium. So as the medium properties do not change along the wire, the effect of temperature increase on electrical properties can be negligible.

In sum, using the presented circuit models and MoTLiM, the effect of the IPG case and the electrode on the tissue heating at the electrode end of an AIMD can be predicted. With these methods, MRI safe AIMDs can be designed. Also, proposed method is capable of solving induced currents on the guidewire. Proposed method can be used for visibility analysis of guidewires and it can be used for prediction of the tip heating and safety monitoring of guidewires. Finally, MoTLiM is used for verification of CTL fixture for measurement of electrical properties of phantom materials.

Bibliography

[1] R. Kalin and M. S. Stanton, "Current clinical issues for mri scanning of pacemaker and defibrillator patients," *Pacing and Clinical Electrophysiology*, vol. 28, no. 4, pp. 326–328, 2005.

[2] OECD(2013), "Medical technologies, in health at a glance 2013: Oecd indicators, oecd publishing," 2013. `http://dx.doi.org/10.1787/health_glance-2013-33-en`.

[3] H. G. Mond and A. Proclemer, "The 11th world survey of cardiac pacing and implantable cardioverter-defibrillators: Calendar year 2009–a world society of arrhythmia's project," *Pacing and Clinical Electrophysiology*, vol. 34, no. 8, pp. 1013–1027, 2011.

[4] V. Acikel and E. Atalar, "Intravascular magnetic resonance imaging (mri)," *Biomedical Imaging: Applications and Advances*, p. 186, 2014.

[5] C. J. Yeung, R. C. Susil, and E. Atalar, "Rf safety of wires in interventional mri: Using a safety index," *Magnetic Resonance in Medicine*, vol. 47, no. 1, pp. 187–193, 2002.

[6] M. K. Konings, L. W. Bartels, H. F. Smits, and C. J. Bakker, "Heating around intravascular guidewires by resonating rf waves," *Journal of Magnetic Resonance Imaging*, vol. 12, no. 1, pp. 79–85, 2000.

[7] F. G. Shellock, "Radiofrequency energy-induced heating during mr procedures: A review," *Journal of Magnetic Resonance Imaging*, vol. 12, no. 1, pp. 30–36, 2000.

[8] P. A. Bottomley, A. Kumar, W. A. Edelstein, J. M. Allen, and P. V. Karmarkar, "Designing passive mri-safe implantable conducting leads with electrodes," *Medical Physics*, vol. 37, no. 7, pp. 3828–3843, 2010.

[9] D. W. Carmichael, J. S. Thornton, R. Rodionov, R. Thornton, A. McEvoy, P. J. Allen, and L. Lemieux, "Safety of localizing epilepsy monitoring intracranial electroencephalograph electrodes using mri: Radiofrequency-induced heating," *Journal of Magnetic Resonance Imaging*, vol. 28, no. 5, pp. 1233–1244, 2008.

[10] P. Nordbeck, F. Fidler, M. T. Friedrich, I. Weiss, M. Warmuth, D. Gensler, V. Herold, W. Geistert, P. M. Jakob, G. Ertl, *et al.*, "Reducing rf-related heating of cardiac pacemaker leads in mri: Implementation and experimental verification of practical design changes," *Magnetic Resonance in Medicine*, vol. 68, no. 6, pp. 1963–1972, 2012.

[11] W. R. Nitz, A. Oppelt, W. Renz, C. Manke, M. Lenhart, and J. Link, "On the heating of linear conductive structures as guide wires and catheters in interventional mri," *Journal of Magnetic Resonance Imaging*, vol. 13, no. 1, pp. 105–114, 2001.

[12] V. Acikel and E. Atalar, "Modeling of radio-frequency induced currents on lead wires during mr imaging using a modified transmission line method," *Medical Physics*, vol. 38, no. 12, pp. 6623–6632, 2011.

[13] R. C. Susil, C. J. Yeung, and E. Atalar, "Intravascular extended sensitivity (ives) mri antennas," *Magnetic Resonance in Medicine*, vol. 50, no. 2, pp. 383–390, 2003.

[14] S. Weiss, P. Vernickel, T. Schaeffter, V. Schulz, and B. Gleich, "Transmission line for improved rf safety of interventional devices," *Magnetic Resonance in Medicine*, vol. 54, no. 1, pp. 182–189, 2005.

[15] O. Ocali and E. Atalar, "Intravascular magnetic resonance imaging using a loopless catheter antenna," *Magnetic Resonance in Medicine*, vol. 37, no. 1, pp. 112–118, 1997.

[16] E. Atalar, P. A. Bottomley, O. Ocali, L. C. Correia, M. D. Kelemen, J. A. Lima, and E. A. Zerhouni, "High resolution intravascular mri and mrs by using a catheter receiver coil," *Magnetic Resonance in Medicine*, vol. 36, no. 4, pp. 596–605, 1996.

[17] A. J. Martin, D. B. Plewes, and R. M. Henkelman, "Mr imaging of blood vessels with an intravascular coil," *Journal of Magnetic Resonance Imaging*, vol. 2, no. 4, pp. 421–429, 1992.

[18] M. Etezadi-Amoli, P. Stang, A. Kerr, J. Pauly, and G. Scott, "Interventional device visualization with toroidal transceiver and optically coupled current sensor for radiofrequency safety monitoring," *Magnetic Resonance in Medicine*, 2014.

[19] M. A. Stuchly, T. W. Athey, G. M. Samaras, and G. E. Taylor, "Measurement of radio frequency permittivity of biological tissues with an open-ended coaxial line: Part ii- experimental results," *IEEE Transactions on Microwave Theory and Techniques*, vol. 82, no. 1, pp. 87–92, 1982.

[20] K. Foster and J. Schepps, "Dielectric properties of tumor and normal tissues at radio through microwave frequencies.," *The Journal of Microwave Power*, vol. 16, no. 2, pp. 107–119, 1981.

[21] J.-Z. Bao, M. L. Swicord, and C. C. Davis, "Microwave dielectric characterization of binary mixtures of water, methanol, and ethanol," *The Journal of Chemical Physics*, vol. 104, no. 12, pp. 4441–4450, 1996.

[22] U. Erle, M. Regier, C. Persch, and H. Schubert, "Dielectric properties of emulsions and suspensions: mixture equations and measurement comparisons.," *The Journal of microwave power and electromagnetic energy: a publication of the International Microwave Power Institute*, vol. 35, no. 3, pp. 185–190, 1999.

[23] Y. Wang, T. D. Wig, J. Tang, and L. M. Hallberg, "Dielectric properties of foods relevant to rf and microwave pasteurization and sterilization," *Journal of Food Engineering*, vol. 57, no. 3, pp. 257–268, 2003.

[24] M. A. El-Rayes and F. T. Ulaby, "Microwave dielectric spectrum of vegetation-part i: Experimental observations," *IEEE Transactions on Geoscience and Remote Sensing,*, no. 5, pp. 541–549, 1987.

[25] T. Jackson, "Laboratory evaluation of a field-portable dielectric/soil-moisture probe," *IEEE Transactions on Geoscience and Remote Sensing,*, vol. 28, no. 2, pp. 241–245, 1990.

[26] J. Baker-Jarvis, E. J. Vanzura, and W. A. Kissick, "Improved technique for determining complex permittivity with the transmission/reflection method," *IEEE Transactions on Microwave Theory and Techniques*, vol. 38, no. 8, pp. 1096–1103, 1990.

[27] M. D. Janezic and J. A. Jargon, "Complex permittivity determination from propagation constant measurements," *IEEE Microwave and Guided Wave Letters*, vol. 9, no. 2, pp. 76–78, 1999.

[28] B. Akin, Y. Eryaman, and E. Atalar, "A method for phantom conductivity and permittivity measurements," in *26th Annual ESMRMB Meeting, Antalya, Turkey*, 2009.

[29] D. Zemann and K. Moertlbauer, "Using transmission line theory to analyze rf induced tissue heating at implant lead tips," *Proceedings of International Society for Magnetic Resonance in Medicine*, 2012.

[30] C. J. Yeung and E. Atalar, "A greens function approach to local rf heating in interventional mri," *Medical Physics*, vol. 28, no. 5, pp. 826–832, 2001.

[31] S. Gabriel, R. Lau, and C. Gabriel, "The dielectric properties of biological tissues: Ii. measurements in the frequency range 10 hz to 20 ghz," *Physics in Medicine and Biology*, vol. 41, no. 11, p. 2251, 1996.

[32] T. W. Hertel and G. S. Smith, "The insulated linear antenna-revisited," *IEEE Transactions on Antennas and Propagation,*, vol. 48, no. 6, pp. 914–920, 2000.

[33] I. B. Akca, O. Ferhanoglu, C. J. Yeung, S. Guney, T. O. Tasci, and E. Atalar, "Measuring local rf heating in mri: Simulating perfusion in a perfusionless

phantom," *Journal of Magnetic Resonance Imaging*, vol. 26, no. 5, pp. 1228–1235, 2007.

[34] D. Shrivastava, T. Hanson, J. Kulesa, J. Tian, G. Adriany, and J. T. Vaughan, "Radiofrequency heating in porcine models with a large 32 cm internal diameter, 7 t (296 mhz) head coil," *Magnetic Resonance in Medicine*, vol. 66, no. 1, pp. 255–263, 2011.

[35] D. M. Pozar, *Microwave Engineering.* John Wiley & Sons, 2009.

[36] R. C. Susil, C. J. Yeung, H. R. Halperin, A. C. Lardo, and E. Atalar, "Multifunctional interventional devices for mri: a combined electrophysiology/mri catheter," *Magnetic resonance in medicine*, vol. 47, no. 3, pp. 594–600, 2002.

[37] D. Shrivastava and J. T. Vaughan, "A generic bioheat transfer thermal model for a perfused tissue," *Journal of Biomechanical Engineering*, vol. 131, no. 7, p. 074506, 2009.

[38] P. Vernickel, V. Schulz, S. Weiss, and B. Gleich, "A safe transmission line for mri," *IEEE Transactions on Biomedical Engineering,*, vol. 52, no. 6, pp. 1094–1102, 2005.

[39] M. E. Ladd and H. H. Quick, "Reduction of resonant rf heating in intravascular catheters using coaxial chokes," *Magnetic Resonance in Medicine*, vol. 43, no. 4, pp. 615–619, 2000.